Seasonal methane accumulation and release from a gas emission site in the central North Sea

S. Mau[1]*, T. Gentz[2], J.-H. Körber[1], M. Torres[3], M. Römer[1], H. Sahling[1], P. Wintersteller[1], R. Martinez[2], M. Schlüter[2], E. Helmke[2]

[1] MARUM – Center for Marine Environmental Sciences and Department of Geosciences, University of Bremen, Klagenfurter Str., 28359 Bremen, Germany

[2] Alfred-Wegener-Institute for Polar and Marine Research, Am Handelshafen 12, 27570 Bremerhaven, Germany

[3] College of Oceanic and Atmospheric Sciences, Oregon State University, 104 Ocean Admin Building, Corvallis, Oregon 97331-5503

* Corresponding author: Susan Mau, e-mail: smau@marum.de

Abstract

Hydroacoustic data document the occurrence of 5 flare clusters and several single flares from which bubbles rise through the entire water column from an active seep site at 40 m water depth in the central North Sea. We investigated the difference in dissolved methane distributions along a 6 km transect crossing this seep site during a period of seasonal summer stratification (July 2013) and a period of well mixed winter water column (January 2014). Dissolved methane accumulated below the seasonal thermocline in summer with a median concentration of 390 nM, whereas during winter, methane concentrations were much lower (median concentration of 22 nM) and punctually elevated due to bubble transport. High resolution methane analysis by an underwater mass-spectrometer confirmed our summer results and were used to document prevailing stratification over the tidal cycle. Although sufficient methane was available, microbial methane oxidation was limited during both seasons. Measured and averaged rate constants (*k'*) were on the order of 0.01 day^{-1}, equivalent to a turnover time of 100 days. Time series measurements indicated a microbial uptake of only 5-6% of the gas after 4 days, and no known methanotrophs and pmoA-genes were detected. Estimated methane fluxes indicate that horizontal transport rapidly disperses dissolved methane, vertical transport becomes dominant during phases of high wind speeds, and relative to these processes, microbial methane oxidation appears to be low. To bridge the discrete field data we developed a 1D seasonal model using available year-long records of wind speed, surface temperature and thermocline depth. The model simulations show a peak release of methane at the beginning of fall when the water column becomes mixed. Consistent with our field data, inclusion of microbial methane oxidation does not change the model results significantly, thus microbial oxidation appears

to be not sufficient to notably reduce methane during summer stratification before the peak release in fall.

1 Introduction

Methane is, after water vapor and CO_2, the most important greenhouse gas. Its concentration has increased by a factor of 2.5 since preindustrial times, from 722 ppb in 1750 to 1800 ppb in 2011 (IPCC, 2013). The total global emission was estimated to be ~550 Tg (methane) yr^{-1} with an anthropogenic contribution of 50 to 65%. Geological sources, which were not considered in IPCC reports previously, are suggested to account for up to 30% of total emissions and include anthropogenic emissions related to leaks in the fossil fuel industry as well as natural geological seeps both terrestrial and marine (IPCC, 2013). An improved emission estimate from marine seeps suggests that these sources contribute ~20 Tg methane yr^{-1}, i.e., 4% of the global emissions, to the atmospheric methane (Etiope et al., 2008).

In general, oceans have been found to be a minor source of methane to the atmosphere, accounting for 2-10% of the global emissions (Bange et al., 1994). A major fraction of the oceanic source (75%) is thought to originate from estuaries, shelf and coastal areas (Bange, 2006; Bange et al., 1994). For example, the European coastal areas were found to emit 0.46-1 Tg yr^{-1}, and thus contribute significantly to the overall global methane oceanic emissions (Bange, 2006). The author, however, points out that this estimate underestimates the coastal input, since fluxes from estuaries and shallow seeps are not adequately represented. Moreover, there is growing evidence that methane release from natural seepages and abandoned boreholes can significantly contribute to the global atmospheric methane emissions, especially from the North Sea (Judd et al., 1997; Rehder et al., 1998; Schroot et al., 2005).

It is important to consider shelf and coastal areas, as they are regions where most organic matter is deposited. Although continental margins account for only 10% of total ocean area and 20% of total ocean primary production (Killops and Killops, 1993), more than 90% of all organic carbon burial occurs in sediments depositing on deltas, continental shelves, and upper continental slopes (Berner, 1989). At these locations, which are also characterized by high sedimentation rates, organic carbon is rapidly buried beneath the sulfate reduction zone, and becomes available to methanogens (e.g. Cicerone and Oremland, 1988). Methane is also generated by thermal breakdown at high temperature and pressure. A significant fraction of the formed methane is oxidized in anaerobic and aerobic sediments (e.g. Boetius et al., 2000; King, 1992), the remaining methane may be transported into the overlying water either dissolved in upwardly advecting pore waters or in case of

oversaturation, in the form of gas bubbles. Because methane is undersaturated in seawater, rising methane bubbles partially dissolve during ascent through the water column (McGinnis et al., 2006), where the dissolved methane may be further consumed by microbial oxidation. Only if this methane survives transport to the mixed layer, can it be transferred to the atmosphere.

Using a bubble dissolution model in combination with acoustic observations of rising bubbles, McGinnis et al. (2006) showed that only bubbles emitted at shallow seeps (<100 m) may reach the atmosphere. Methane rich bubbles from deeper seeps fully dissolve in the ocean. Model simulations based on methane concentrations, oxidation rates, and current records of two plumes observed in the Santa Barbara Basin indicate that half of the dissolved methane reaches the atmosphere and the other half is microbially oxidized of the shallow plume whereas the deeper plume is mostly oxidized (Mau et al., 2012). Thus, depending on the emission depth, methane remains in the ocean and can be microbially oxidized.

Shallow seeps thus are likely more important contributors to atmospheric methane. However, even at shallow seeps, density stratification may limit the vertical transport. For example, at the 70 m deep Tommeliten area in the North Sea, less than ~4% of the gas initially released at the seafloor reaches the mixed layer during summer, because a seasonal thermocline constrains methane transport to the atmosphere (Schneider von Deimling et al., 2011). Summer stratification traps methane beneath the thermocline, some of which may be consumed by microbial oxidation, and some will be released in the fall during first storm events. In order to investigate the seasonal cycle of methane in the North Sea, we studied a shallow seep area both during summer (July 2013) when the water column was stratified, and in winter (January 2014) when the water column was well mixed.

1.1 Study Site

The study site is situated in an area of active gas venting above a shallow gas reservoir in the central North Sea. The gas vents are located in the Netherlands sector, license block B13 (Fig. 1). They occur at shallow water depth (< 45 m) in a flat region that lacks any morphological expression typical of seep structures (Schroot et al., 2005). These seeps are likely sourced from a biogenic methane reservoir ($\delta^{13}C$ values of -80‰ VPDB) of Pliocene to Pleistocene age, which lies 600-700 m below the seafloor. Patches of gas saturated sediments between the gas reservoir and the seafloor have been imaged in seismic data. These data plus observations of separate bubble streams in the water column and rapidly decreasing methane concentrations in cores with distance from the vent site led Schroot et al. (2005) to describe our study site as a leaking gas reservoir with laterally discontinuous seepage.

105
106 The seeps are located in the central North Sea, south of Dogger Bank, a sandbank with water depth
107 20 m shallower than in the surrounding sea. Water masses from the north (Atlantic Water) and south
108 (Straits of Dover) meet (Kröncke and Knust, 1995) in this central area, where the general
109 anticlockwise circulation along the coasts of the North Sea becomes weak and varied (Fig. 1,
110 Howarth, 2001). The water above the sandbank is well-mixed throughout the year in contrast to the
111 deeper waters surrounding the bank that become stratified during spring and summer. The front,
112 where these waters encounter, bifurcates around the Dogger Bank and the location of the front is
113 influenced by tidal current speed. Generally, tides have the strongest influence on currents in this
114 region, followed by wind forcing (Howarth, 2001; Otto et al., 1990; Sündermann and Pohlmann,
115 2011).
116
117 Seasonal temperature stratification is a common feature in this and other shelf seas, and it separates
118 high-light and low-nutrient surface water from low-light and high-nutrient bottom water. Even
119 though in some shelf areas, the tidal energy is sufficient to overcome stratification, models by
120 Pingree and Griffiths (1978) and Holt and Umlauf (2008) indicate that our study area is situated in a
121 stratified region, east of the tidal front that surrounds the shallowest part of the Dogger bank. Thus,
122 during spring and summer, the water column over the seeps investigated here, remains stratified
123 over the course of a tidal cycle.
124
125 2 Methods
126 All data used in this study was collected during two cruises with *RV Heincke*. The first cruise (HE406)
127 was conducted during summer 2013 (20.-24. July), the second cruise (HE413) during winter 2014
128 (13.-22. January).
129
130 2.1 EM710 flare imaging
131 During the winter cruise, we used a Kongsberg EM710 multibeam echosounder to map active gas
132 emissions in the study area (Fig. 2). For the precise localization of individual flares, i.e., bubble
133 streams in an echogram, the water column data were post-processed using the Fledermaus tools
134 FMMidwater, DMagic, and the 3D Editor (© QPS). The origin of individual flares was identified as the
135 point of highest amplitudes near the seafloor. The coordinates of these points were extracted using
136 the FMGeopicker and subsequently plotted on top of the bathymetry using ArcGIS 10.2 (©ESRI).
137
138 For visualization of flare deflections and bubble rising heights, selected flares were extracted from
139 the water column data as point data and edited using the 3DEditor of DMagic. The processed flares
140 were plotted over the bathymetry data in a 3D-view.

2.2 Water column sampling

To identify the size and magnitude of the dissolved methane plume generated by the bubble discharge, seawater was sampled along a transect crossing the active gas emission sites (Fig. 2). The transect, which extends 3 km to the east and 3 km to the west from a bubbling location (cluster 1 in Fig. 2) was sampled twice, once in summer 2013 and once in winter 2014. In both cases, the eastern sector (5 stations) was sampled on one day (~3 h) and the western sector (5 stations) on another day (~3 h), so that the center stations was sampled twice.

Water samples were collected with a CTD/bottle rosette for methane concentration, methane oxidation rate, and molecular analyses. The rosette was equipped with twelve 5 L Niskin bottles, a Sea-Bird SBE 911 plus CTD, and an SBE 43 oxygen sensor for online monitoring of salinity, temperature, pressure, and dissolved oxygen. The data are archived in PANGAEA (doi:10.1594 / PANGAEA.824863 and doi:10.1594 / PANGAEA.832334). Twelve different water depths were sampled at each station for methane concentration analysis and 5 water depths for methane oxidation rates. Additional casts were conducted to sample sufficient water for molecular analyses.

2.2.1 Methane concentration

For methane concentration analysis, samples were collected in 60 ml crimp-top glass bottles. All sample bottles were flushed with 2 volumes of water and filled completely to eliminate bubbles. Bottles were immediately capped with butyl rubber stoppers and crimp sealed. After adding 0.2 ml of 10 M NaOH to stop any microbial activity, a 5 ml headspace of pure N_2 was introduced into each bottle as described in Valentine et al. (2001) and the samples were stored at 4 °C. One to two aliquots of the headspace were analyzed to determine methane concentrations using a gas-phase chromatograph equipped with a flame ionization detector. Analyses were performed both on board and post cruise. Replicate analyses of samples yielded a precision of ± 5%.

2.2.2 Methane oxidation rates

Methane oxidation (MOx) rates were determined from ex situ incubations of water samples in 100 ml serum vials. Sampling and incubations were performed as described in Mau et al. (2013). Briefly, duplicate samples were collected: the set of samples taken at all stations was treated with 50 µl of ^{3}H-labeled methane (160–210 kBq) in N_2, and a second sample set, which was collected at 5 stations in July 2013, was treated with 10 µl of ^{14}C-labeled methane (12–15 kBq). After shaking the bottles to equilibrate the tracer with the water, the samples collected in summer 2013 were incubated at 10 °C and those collected in winter 2014 at 9 °C. All samples were incubated in the dark for 24 h. After

incubation, the total activity (^{3}H-CH_4 + ^{3}H-H_2O) in 1 ml aliquots was measured by wet scintillation counting, and the activity of ^{3}H-H_2O was measured after sparging the sample for >30 min with N_2 to remove excess ^{3}H-CH_4. Incubations with ^{14}C-CH_4 were terminated by injecting 0.5 ml of 10 M NaOH. A 5 ml headspace was then added so that the remaining ^{14}C-CH_4 accumulated in the headspace, while produced ^{14}C-CO_2 and ^{14}C biomass was trapped in the aqueous NaOH solution. ^{14}C-CH_4 in the headspace was combusted to ^{14}C-CO_2, and ^{14}C-CO_3^{2-} was converted to ^{14}C-CO_2 through acidification with HCl. The produced ^{14}C-CO_2 was trapped in a solution of methoxyethanol and phenylethylamine, and the radioactivity was measured by wet scintillation counting.

MOx rates were calculated assuming first-order kinetics (Reeburgh et al., 1991; Valentine et al., 2001):

$$MOx = k'[CH_4] \quad (1)$$

where *k'* is the effective first-order rate constant calculated as the fraction of labeled methane oxidized per unit time, and [CH_4] is the in situ methane concentration. To verify first order kinetics we conducted time series incubations and measured the tracer consumption after 1, 2, 3, and 4 days.

In addition, control samples were frequently taken and poisoned immediately after the addition of the tracer. The mean ($\bar{x}$) and standard deviation (*s*) of all controls sampled during a cruise were calculated and the limit of detection (LOD) was set as:

$$LOD = \bar{x} + 3s \quad (2)$$

The *LOD* was 0.02 nM day^{-1} for the summer 2013 survey, 0.09 nM day^{-1} for the winter 2014 survey, and 0.0005 nM day^{-1} for the ^{14}C-methane survey in summer 2013.

The MOx values were also corrected for differences between in situ and incubation temperatures (Supplementary Material 1).

2.2.3 Analysis of bacterial communities

The composition of the bacterioplankton assemblages was examined using denaturing gradient gel electrophoresis (DGGE) based on the 16S rRNA gene as described in Mau et al. (2013). In short, immediately after sampling, 8 L of water were filtered and bacterial cells were concentrated on Nuclepore filters (0.2 µm pore size). The filters were stored on board at -20 °C and at -80 °C post

cruise. DNA was extracted by an UltraClean Soil DNA Kit (MoBio Laboratories, USA). 16S rRNA gene specific PCR was conducted using the forward primer GM5 plus GC-clamp and the reverse primer 907RM (Muyzer et al., 1993) under conditions described by Gerdes et al. (2005). The PCR products (ca. 500 bp) were analyzed by DGGE according to the protocol of Muyzer et al. (1993). Clearly visible bands of the DGGE gels were excised from the gel. The DNA was reamplified by PCR (Gerdes et al., 2005) and sequenced. The 16S rRNA gene sequences were taxonomically assigned by SILVA Online Aligner (Pruesse et al., 2012).

The presence of methane-oxidizing bacteria in the communities was checked by searching for genes encoding the particulate methane monooxygenase (*pmoA*), a key enzyme of methanotrophs (McDonald et al., 2008). The *pmoA*-gene-specific PCR reaction was conducted by using the primer set "pmoA" and amplification conditions described in McDonald and Murrell (1997).

2.3 Methane concentration analysis by underwater mass-spectrometry (UWMS)

In addition to the conventional methane analysis, in situ methane concentrations were detected and quantified with an UWMS (Inspectr200-200, Bell et al., 2007; Gentz et al., 2013; Schlüter and Gentz, 2008; Short et al., 2001; Wenner et al., 2004). The fast sampling frequency (≤ 2 s) of the UWMS allows mapping and quantification of methane in much higher resolution than the commonly used CTD/rosette-sampling technique. The instrument consists of a membrane inlet system (MIS), an Inficon (Bad Ragaz, Switzerland) Transpector CPM 200 quadruple mass spectrometer, a Varian (Palo Alto, USA) turbo pump, a roughing pump, a peristaltic pump (KC Denmark), an embedded PC, and a microcontroller. The UWMS was partly redesigned to include a cooling system (Ricor, K508), which lowers the detection limit for methane to 16 nM. The cooling system and the improvement of the detection limit are described in detail by Gentz and Schlüter (2012) and Schlüter and Gentz (2008). For reproducible gas permeation through the MIS, water is constantly heated to a steady temperature of 50°C and pumped at a flow rate of 3 ml min^{-1} along the membrane by an external peristaltic pump.

The UWMS was deployed above the central gas seeps (cluster 1, Fig. 2) on 21.07.2013 (16:31 – 22:32 UTC) at five different water depths: just above the seafloor, 35 m, 28 m, 25 m, and 10 m. When the system had reached the respective depth, the research vessel moved slowly along a rectangular transect (~125 m S-N, ~150 m E-W, Fig. 2) surrounding the flares of cluster 1 (4°5.44'N, 55°18.36'E) and towed the UWMS, which continuously measured the methane concentrations. Each of the depth transects took about an hour and recorded 400-800 methane concentration values.

246 2.4 Estimation of methane fluxes

247 Advection, horizontal and vertical turbulent diffusion, sea-air flux, and microbial oxidation were
248 quantified for the upper (0-30 m) and lower water column (30-40 m) during summer stratification
249 (July 2013) and for the entirely mixed water column (0-40 m) in winter (January 2014).

250

251 The advective flux (*ADV*) was calculated by multiplying methane concentration (*C*) and current
252 velocity (*v*):

253

254 $$ADV = vC \quad (3)$$

255

256 Methane concentrations were averaged above and below the thermocline in the case of the summer
257 results and throughout the water column in the case of the winter results. Current velocities refer to
258 the resultant velocities calculated from the u and v component of the velocity vectors
259 (Supplementary Material 2 and 3) and were averaged over the time period of sampling. The current
260 data were provided by the *Bundesamt für Seeschifffahrt und Hydrographie* (BSH)
261 (www.bsh.de/de/Meeresdaten/Vorhersagen/Vorhersagemodelle/index.jsp) and were modelled
262 using wind and air temperature forecasts.

263

264 Turbulent horizontal and vertical diffusion (*Diff*) were calculated with Fick's first law of diffusion as
265 described in Mau et al. (2012):

266

267 $$Diff = D\left(\frac{\partial C}{\partial x}\right) \quad (4)$$

268

269 where *D* is the horizontal or vertical diffusion coefficient in $m^2\ s^{-1}$. $\delta C/\delta x$ is the spatial concentration
270 gradient in nM m^{-1}, estimated between the center and the outermost stations in the case of
271 horizontal diffusion calculation, and the concentration gradient between the lower and upper water
272 column in the case of vertical diffusion, calculated only for summer 2013.

273

274 D_h, the horizontal diffusion coefficient, can range between 0.1 and 1000 $m^2\ s^{-1}$ (Largier, 2003;
275 Sundermeyer and Price, 1998) depending on the proximity to land. As the study area is located more
276 than 230 km from shore, we used a D_h of 1000 $m^2\ s^{-1}$ for our calculations. The vertical turbulent
277 diffusion coefficient (D_v) can vary between 10^{-3} and 10^{-6} $m^2\ s^{-1}$ depending on the energy in the water
278 column (wind, tides, etc.) and stratification (Denman and Gargett, 1983; Wunsch and Ferrari, 2004).
279 As a first approximation, we used 10^{-4} $m^2\ s^{-1}$, which is a common cited value across the thermocline.
280 The vertical eddy diffusion was estimated for all vertical profiles (all 10 CTD-stations).

The sea-air flux was calculated as:

$$SAF = k_W(C_W - C_A) \quad (5)$$

where k_W is the gas transfer velocity in cm h^{-1}, C_W is the measured concentration of methane and C_A is the methane concentration in atmospheric equilibrium, both in nM. We calculated k_W, which depends on wind speed and the temperature-dependent Schmidt number of the gas, using parameterization developed by McGillis et al. (2001). Wind speed was recorded 22 m above sea level onboard and corrected to the standard height of 10 m. C_A was derived using the Bunsen solubilities given by Wiesenburg and Guinasso (1979) and measured ocean temperature and salinities. The sea air flux was calculated for surface water samples of all 10 stations sampled in summer 2013 and winter 2014.

The oxidative loss (OL) was calculated by depth integration of the MOx rates:

$$OL = \overline{x}_{MOx} z \quad (6)$$

where $\overline{x}_{MOx}$ is the averaged MOx rate in nM day^{-1} over the depth interval z in m. The depth interval is defined by the water stratification in the case of summer 2013 and covers the entire water depth in the case of winter 2014. Integration was done for all vertical profiles.

2.5 Seasonal model

A non-steady state, 1D-model was developed to investigate the temporal evolution of methane over a year. We considered an entirely mixed water column during the winter month, stratification development during spring that lasted until early fall when the entire water column becomes mixed again. Hence, we considered one water layer during fall-winter (0-40 m) and two layers (upper and lower water column) during spring and summer. The initial model configuration was defined by the dissolved methane concentration observed in January 2014 (17 nM, excluding punctual high concentrations due to bubbles) and the transport and loss quantities calculated for the mixed water column condition in this month. We set the methane flux from the seafloor to be equal to the *SAF* estimate of January 2014. In daily time steps, the *SAF* and the vertical eddy diffusion were calculated using Eq. 3 and 4 (above) and based on the amount of methane obtained in the previous time step. The parameters: mixed layer depth, wind speed, and surface water temperature were kept constant over a month, but then adjusted to the conditions of the following month. The mixed layer depth

was determined from archived CTD-profiles (Pangaea) collected in an area extending from 3-6°E and 54-56°N. Monthly mean wind speed was taken from the web-site: www.windfinder.com of the Ameland Oil Platform (mean of data from Aug. 2010-Mar. 2014) and Forties/North Sea (mean of data from Dec. 2012- Mar. 2014). Surface water temperatures were provided by the BSH.

3 Results

3.1 Seep locations

Echosounder data indicate bubble emission in the area of the sampled transect (Fig. 2). The center station was located at a known gas bubble emission site or flare cluster, where several bubble streams occur in close proximity to each other. We observed an additional four flare clusters near the western sector of the transect, which displayed a similar seepage intensity as at the central seep site. In contrast, no additional flares were found in the area of the eastern sector. Although echosounder data point to bubbles rising to, or close to, the sea surface, no bubbles were visually identified at the sea surface due to rough sea state in winter 2014, however, surfacing gas bubbles were visually documented when the sea was calm in summer 2013. Seepage intensity showed no obvious variation related to tidal cycles, i.e., pressure variations due to high or low tides, rather, seeps were found to be active during all survey crossings.

3.2 Oceanographic setting

In summer (July 2013) a seasonal thermocline separated surface (0-30 m) from bottom water (30-42 m; Fig. 3). The surface water consisted of a 10 m thick mixed layer below which the temperature decreased stepwise from 17.5 to 7°C in 30 m. Lower salinity was observed in 15 and 25 m depth, which departed from the general 34.55. The stepwise decrease in temperature and the salinity variations indicate the successive development of several pycnoclines driven by increasing sea surface temperatures and less wind activity in spring and summer. The oxygen concentrations increased from 220 µM at the surface to 240 µM at 30 m. In contrast to the surface water, the bottom water had a homogeneous temperature of 7°C, a salinity of 34.63 PSU and contained less oxygen (190 µM).

In winter (January 2014) the entire water column was mixed (Fig. 3). The water had a temperature of 7°C, a salinity of 34.85 PSU, a density of 27.3 kg m^{-3}, and oxygen concentrations of 280 µM.

Modelled current data indicate a dominant north-west transport with velocities ranging between 0.06 and 0.27 m s^{-1} (resultant velocity). In summer, the eastern part of the transect was sampled when currents were directed to the north-west with an average velocity of 0.24 m s^{-1} and the

western part was sampled when currents turned from north-west to south-west with an average velocity of 0.19 m s^{-1}. In winter, the eastern part of the transect was sampled when water moved north-east turning north-west with an average velocity of 0.22 m s^{-1} and the western part was sampled when water also turned from north-east to north-west, but with an average velocity of 0.1 m s^{-1}.

3.3 Methane concentrations

Consistent with the two layer structure observed by the temperature/salinity data, methane concentrations in summer 2013 also show a two layer distribution, with higher concentrations in the bottom water relative to the surface values (Fig. 4A). Methane concentrations in the surface water range from 3.9-517.8 nM with a median of 32.5 nM. Methane concentrations in the bottom water range between 39.7 and 1627.7 nM with a median of 390.6 nM. Highest concentrations in the surface water were found near the center station (170 nM), which decreased to the outermost stations (to the west to 96 nM and to the east to 13 nM). However, the decrease is not continuous due to the presence of bubble emission sites in the area. Similarly, in the bottom water the highest methane concentrations were found at the center station (600-700 nM) decreasing unevenly towards the outmost stations (200-300 nM). In both layers the methane concentrations exceed the background concentration of ~20 nM as measured at a reference station, which was located 32 km from the central station (Supplementary Material 4), and reported methane concentrations in Grundwald et al. (2009). Even this background value is already oversaturated with respect to the atmospheric equilibrium concentration of 2.3-2.9 nM (at the relevant T /S conditions, Wiesenburg and Guinasso, 1979).

In winter 2014, much lower methane concentrations were found (Fig. 4B). Highest values were observed near the center site with concentrations of up to 656.6 nM. But such high concentrations decreased rapidly horizontally (within 1 km) and were not encountered during repeated measurements at the same location. The median of all methane concentration measurements along the transect is 22.4 nM, which is only slightly above the regional background concentration. In general, methane concentrations indicate a patchy distribution as expected in an active seep area.

3.4 UWMS methane concentrations

During the cruise in summer 2013, the UWMS was deployed in the vicinity of gas flare cluster 1 (Fig. 2). Because the instrument was towed close to several bubble streams, the recorded methane concentrations range over three orders of magnitude, from 0 to 2127 nM in surface water (transects in 10 m, 25 m, 28 m) and from 259 to 2213 nM in the bottom water (transects in 30 m and 40 m) (Fig.

5). Nonetheless, the general pattern of lower methane concentrations in the surface and higher concentrations in the bottom water observed by conventional methods (see section 3.3) is also apparent in the UWMS-data. The median values of the records in 10 m, 25 m, and 28 m water depth range from 54 to 402 nM and in 30 m and 40 m depth, the medians range from 512 to 793 nM.

The UWMS measured the methane during ebbing tides, where water levels fell from 0.18 to -0.27 m, whereas CTD/rosette samples were collected during rising tides, when sea level height increased from -0.21 to 0.06 m and from 0.04 to 0.16 m (Supplementary Material 5). Again, the general pattern of lower concentrations in the surface and higher ones in the bottom water was apparent in all stations, even though methane data were obtained during different tidal phases.

3.5 Methane oxidation

Similar to the distribution of methane and co-located oceanographic data, MOx rates in summer 2013 show a two layer pattern whereas MOx measured in winter 2014 are uniform throughout the water column (Fig. 6 A, B). In summer, significantly less methane was oxidized in the surface water relative to the bottom water. In the surface waters MOx-rates ranged between 0.04 and 92.64 nM day^{-1} with a median of 0.10 nM day^{-1} and in the bottom water between 1.60 and 840.93 nM day^{-1} with a median of 3.99 nM day^{-1}. The total range of both layers (0.04- 840.93 nM day^{-1}) exceeds the range of MOx-rates observed during the winter survey (0.09-8.72 nM day^{-1}). The median of all MOx-rates measured in January 2014 was 0.24 nM day^{-1}.

Time series and ^{14}C-methane tracer incubations indicate a slow oxidation rate of methane over time. Although the methane concentrations greatly differ during both seasons, only 5-6 % of the ^{3}H-methane tracer was utilized during 4 day of incubation (Fig. 6D). In the ^{14}C-methane tracer experiments, a significantly higher concentration of methane is added to the sample relative to the ^{3}H-methane tracer additions (Mau et al., 2013). However, even the elevated methane additions did not lead to a higher methane utilization. The MOx-rates determined using ^{14}C-methane tracer additions range from 0.0009 to 0.04 nM day^{-1} with a median of 0.003 nM day^{-1} in the surface water (Fig. 6C). In the bottom water, the values range from 0.05 to 0.53 nM day^{-1}, with a median of 0.16 nM day^{-1}. Even though the ^{14}C-MOx-rates were lower than the ones obtained with the ^{3}H-methane tracer, in both cases the two layer structure was obvious for the summer 2013 situation.

3.6 Microbial communities

Molecular samples taken in summer 2013 show also a difference between surface and deep waters, whereas winter 2014 samples indicate a homogeneous distribution of microorganisms (Fig. 7, Tab.

1). In summer 2013, different DGGE banding patterns reveal the changes in microbial communities with depth. The surface water samples showed two strong bands (Fig. 7, bands 6, 7) that could be affiliated to the *Rhodobacteraceae* and two bands that could be assigned to the *Cyanobacteria / Synechococcus* clade (8, 9). The middle and bottom water samples were characterized by a strong chloroplast band (2), but also showed bands affiliated to the *Rhodobacteraceae* (5, 6). In the bottom water samples of the central station, we found an additional band, assigned to *Pseudoalteromonas* (10). The gel pattern of the winter samples showed no significant bands. The sequences of the faint bands excised were of low quality. Only two of the bands could be assigned to the *Rhodospirillaceae* (12, 13).

Neither the summer nor the winter bacterial communities exhibited known methanotrophic bacteria, even though the samples originate from an actively gas venting area. The absence of methanotrophic bacteria was further supported by the negative results of the pmoA-PCRs that targets a methanotroph molecular marker gene.

4 Discussion

4.1 Distribution of methane in summer and winter

Our highest dissolved methane concentrations measured in the bottom water reach magnitudes similar to those observed at other shallow seep sites (Tab. 2). Our highest value of 1627.7 nM is comparable to measurements near the Coal Oil Point seep field, Santa Barbara Basin, California (up to 1900 nM, Mau et al., 2012), and it is higher than methane concentrations reported for the Tommeliten, North Sea (268 nM, Schneider von Deimling et al., 2011), and offshore Svalbard, west of Prins Karls Forland (524 nM, Gentz et al., 2013).

Even though gas bubbling was observed at the sea surface in summer months, the dissolved methane at these and also at other vent sites is trapped beneath a thermocline or halocline, which hampers further ascent of the dissolved methane to the atmosphere. The studied seeps are located at a depth of 40 m and the dissolved methane plume was found beneath a seasonal thermocline. At the Tommeliten seep site, the methane plume was also observed beneath the seasonal thermocline (Schneider von Deimling et al., 2011) whereas the methane plume originating from the 245 m deep seeps offshore Prins Karls Forland was confined to water depths beneath a local halocline (Gentz et al., 2013). In the Baltic Sea, summer stratification also leads to accumulation of methane below the thermocline (Gülzow et al., 2013). At all these sites, an enhanced release of methane to the atmosphere is thought to occur upon erosion of stratification. In contrast, the dissolved methane plume originating from seeps situated between 5 and 70 m at the Coal Oil Point is dispersed above

456 the thermocline within the mixed layer (Mau et al., 2012), and as such is not controlled by seasonal
457 stratification patterns.
458
459 Trapping and accumulation of dissolved methane beneath a thermocline is also well documented in
460 lakes and freshwater reservoirs, where thermal stratification separates methane-poor, surface water
461 from the methane-rich, but anoxic, bottom water in e.g. a shallow floodplain lake in south-eastern
462 Australia (Ford et al., 2002), in a polyhumic lake in southern Finland (Kankaala et al., 2007), in the
463 subtropical Lake Kinneret in Israel (Eckert and Conrad, 2007), and in eight freshwater reservoirs in
464 India (Narvenkar et al., 2013). The accumulated methane is released when water starts mixing driven
465 by enhanced wind forcing and lower temperatures.
466
467 Our results verify the assumption that in a seasonal stratified system, no methane accumulation
468 occurs in winter, when the water column is well mixed as indicated by vertical profiles of
469 temperature, salinity, and oxygen. During our winter field program, methane concentrations were
470 found to deviate only due to bubble ascent and were otherwise low and constant throughout the
471 water. The median winter concentration of 22 nM is similar to the background methane
472 concentrations of 20 nM reported by Grunwald et al. (2009) for the German Bight, but the
473 concentration is elevated relative to water originating from the Atlantic Ocean, which carries 2.5-3.5
474 nM of methane (Rehder et al., 1998) and to the methane background concentrations of <5 nM at
475 Tommeliten (Niemann et al., 2005; Schneider von Deimling et al., 2011).
476
477 4.2 Low methane oxidation
478 Measured MOx-rates at our study site lie at the upper end of MOx-rates previously reported, which
479 span over six orders of magnitude from 0.001-1000 nM day^{-1} (Tab. 2 and summarized in Fig. 1 in Mau
480 et al., 2013). The rates measured in deep water samples during summer (median 3.9 nM day^{-1}, up to
481 840 nM day^{-1}) equal those observed in the Gulf of Mexico after the Deepwater Horizon event
482 (median 10 nM d^{-1}, up to 820 nM day^{-1}) (Valentine et al., 2010). Even winter time rates are high in
483 comparison to rates measured in the Eel River Basin, an area of hydrate dissociation (Valentine et al.,
484 2001) and match rates of the Coal Oil Point seep field in the Santa Barbara Basin (Mau et al., 2012;
485 Pack et al., 2011).
486
487 However, we note that in spite of the reported high MOx values, detailed analysis of the data reveals
488 an overall low activity of methane oxidizing microorganisms. This apparent contradiction arises from
489 the fact that the MOx-rate of a given sample is traditionally calculated by multiplying methane
490 concentration with the fraction of the tracer converted per unit time, i.e., *k'* - the first order rate

constant. At a given *k'* value changes in methane concentrations yield MOx-rates that are low or high depending on whether methane concentrations are low or high. Thus high MOx-rates might just reflect high methane concentrations, and not necessarily a rapid turnover rate. The constant *k'* provides an indication of the relative activity in a water sample (Koschel, 1980), but it cannot be viewed independently from methane concentration, as *k'* is derived from tracer conversion in a sample with ambient methane concentration.

Alternatively, the MOx-rate can be plotted against methane concentration, following the approach used by Michaelis Menten (MM) kinetics to describe the rate of a first order enzymatic reaction that depends on one substrate, by relating the reaction rate (*V*) to the substrate concentration (*S*) (Fig. 8). The model takes the form of the equation:

$$V = v_{max} \frac{S}{(K_m + S)} \quad (7)$$

where v_{max} is the maximum uptake rate and K_m is the concentration at which the reaction rate is half of v_{max}. As illustrated in Fig. 8, the enzymatic uptake can be very rapid as soon as methane is available and levels off when enzyme saturation is reached (low K_m and high v_{max}, MM-kinetics 1). However, in some systems the uptake can be very slow, and enzyme saturation is reached at very high methane concentrations (high K_m and low v_{max}, MM-kinetics 2). K_m values of cultured and uncultured soil methane oxidizing bacteria range between 0.8-12 µM (Baani and Liesack, 2008; Bender and Conrad, 1993). For v_{max}, we used MOx-rate maxima reported for oceanic environments, which range between 100-1000 nM day^{-1} (Mau et al., 2013). Using these wide data ranges, we depict the predictive behavior using both end-member for MM kinetics. Apart from 7 data points, which were collected in the bottom water close to flare cluster 1 (stations S12 and S13, Fig. 2), all other data points are close to a curve that follows MM-kinetics 2, with high K_m value and low v_{max}, hence pointing to a generally slow uptake and oxidation of methane.

As all methane concentrations of our data are below K_m, we can derive an overall *k'* value from the slope of the linear regression (Fig. 8), which for our case is 0.01 day^{-1}. As expected this value matches the majority of the measured *k'* values (median of summer data: 0.02 day^{-1}, median of winter data: 0.01 day^{-1}, Supplementary Material 6) as well as the value *k'* derived from the time series incubations (0.01 day^{-1}, n=4). We pose that, rather than using MOx-rates, or *k'* values from individual samples, a fit to the entire data set provides an effective way to generate an overall parameter *k'*, which best reflects the ecosystem microbial activity. The inverse of the modelled *k'* gives a turnover time of 100 days suggesting a rather low activity of methane-oxidizing bacteria in both summer and winter.

The low activity of methane oxidizing microorganisms is further supported by time series experiments, ^{14}C-methane spike experiments, and molecular analysis of filtered matter from seawater. Time series incubations show a slow uptake of methane over time, solely 5-6% of the added ^{3}H-methane-tracer was converted after 4 days. Even when we spiked the sample with elevated ^{14}C-methane concentrations of 400-500 nM, there was no additional substrate utilized after incubation for one day, indicating that methane oxidizing microorganisms cannot rapidly consume the additional methane. Consistently, DGGE and *pmoA* analysis did not reveal the presence of any known methanotrophic bacteria or *pmoA*-genes. Either methanotrophs were only present in low numbers and/or poorly matched to the used PCR primers and, thus, were not detected (Hansman, 2008). Other observations in shallow marine waters (< 200 m) in the Pacific, Atlantic, and the Gulf of Mexico show also that canonical methanotrophs were not detectable, but revealed novel sequences closely related to those coding for methane monooxygenase (Elsaied et al., 2004; Tavormina et al., 2008; Tavormina et al., 2013; Valentine, 2011; Wasmund et al., 2009), an enzymatic hallmark of aerobic methanotrophs.

4.3 Transport is faster than methane oxidation

Although a part of the methane flux to the atmosphere is supported by direct bubble-transport, a component that is being constrained by video observations and gas bubble samples (T. Gentz, personal communication, 2014), here, we focus on the fate of the dissolved methane fraction. When methane enters the water column, it is transported by ocean currents and spreads by horizontal and vertical eddy diffusion. Dissolved methane can then support methane oxidizing microorganisms and if water with methane concentrations higher than saturation reach the mixed layer, methane will be transferred into the atmosphere. In order to evaluate the relative importance of these transport and loss processes, we estimated the advective transport, the horizontal and vertical eddy diffusion, sea-air flux, and integrated the MOx-rates over the water depth (see methods). All fluxes were estimated in units of nmol m^{-2} s^{-1}. As shown in Fig. 9, we estimated summer fluxes for the bottom (30-43m) and surface waters (0-30 m), using data collected in July 2013, and winter fluxes for the entire unstratified water column (0-42m) using data from January 2014. The results show that advective transport and the horizontal eddy diffusion are the dominant processes rapidly transporting and diluting the emitted methane. The loss processes, i.e., sea air flux and microbial oxidation, are more than 4-orders of magnitude lower than these horizontally directed processes. Our flux estimates revealed that in summer more methane is transported via vertical diffusion into the surface water than is oxidized in the bottom water. In the surface water, 50% is oxidized and the other 50% is transferred into the atmosphere. In winter, the sea air flux removes more methane from the water

column due to increased wind speed. Overall the flux estimates indicate that diffusion (dilution of the methane rich water with background ocean water) outcompetes microbial methane oxidation.

All of these flux estimates are snapshots based on a few discrete samples and may vary by up to one order of magnitude. The estimates were determined as described by Mau et al. (2012), which includes a detailed discussion of the uncertainties associated with the calculations. Briefly, the uncertainty originates from the precision of the different measurements, assumed diffusion coefficients, and the parameterization of the gas transfer velocity. The uncertainty does not include any possible variations during the 3 h of sampling. However, as the overall environmental setting will remain constant, e.g. with the establishment of a seasonal thermocline and higher wind speed during winter, the trend indicated by the flux comparison persists despite the uncertainties. Advection and horizontal diffusion of methane will remain consistently higher than vertical diffusion and methane oxidation.

Our flux estimates suggest that microbial oxidation is of minor importance in the central North Sea. Particularly during periods of high wind speed (fall and winter), more methane reaches the atmosphere than is oxidized in the water. In summer when lower wind speeds prevail, methane oxidation is similar in magnitude to the gas transfer to the atmosphere. Our findings are similar to those reported by Scranton and McShane (1991), who conclude that methane oxidation constitutes a relatively small sink for methane in the Southern Bight of the North Sea (0.00023-0.3 nM day^{-1}), relative to methane losses to the atmosphere (0.00026-7.5 nM day^{-1}), which are highest during periods of high wind speed. The data are consistent with estimates for the shallow Coal Oil Point methane plume in the Santa Barbara Basin (Mau et al., 2012). There, 0.05 mol day^{-1} are oxidized in the surface water and 0.03 mol day^{-1} are transferred to the atmosphere.

4.4 Modeled methane accumulation and flux to the atmosphere over a year

To extend our inferences based on 2 field programs to seasonal changes over an entire year, we developed a 1D model using wind speed, sea surface temperature, and the depth of the mixed layer defined by the depth of the thermocline. CTD data of the surveyed region were used to specify the monthly development of the mixed layer depth, which develops in May and deepens until the entire water column becomes mixed in September (Fig. 10D). The model focused on the sinks of dissolved methane: sea air flux and microbial methane oxidation.

Three simulation were run. The first simulation included solely the vertical transport (sea air flux and vertical eddy diffusion during stratification), the second tested the uncertainty of the first simulation

due to the most unspecified parameter, *Dv*, and the third simulation included the microbial methane oxidation (Fig. 10A-C).

Model results of the first simulation, which do not include methane oxidation, illustrate the seasonal changes in methane concentrations. With decreasing wind speed in spring, methane concentration slowly rise in the water column; at the onset of stratification, most of the dissolved methane accumulates in the bottom water, leaving the surface water as the only source of methane to the atmosphere and, thus, reducing the methane concentrations in the surface water. As the concentration gradient between bottom and surface increases, more methane is transferred to the surface water by vertical eddy diffusion; that in combination with lower wind speeds in the summer cause methane concentrations to increase in the surface water. In late summer, beginning of fall, the mixed layer depth deepens due to increased wind forcing. Surface and bottom waters become mixed, which leads to a peak in methane concentration in the entire water column. This is transferred to the atmosphere by sea air exchange. Due to prevailing high wind speeds in fall and winter, methane concentrations rapidly decrease to a background concentration level of 20 nM.

The first simulation is greatly dependent on the vertical diffusion coefficient *Dv*. This parameter could be one order higher (10^{-3} m^2 s^{-1}) due to shallow water depth or one order lower (10^{-5} m^2 s^{-1}) due to low wind speed especially in summer (Denman and Gargett, 1983; Wunsch and Ferrari, 2004). For example, during the first sampling period in July 2013 a wind speed of 2-5 m s^{-1} was recorded whereas the average value used for the month July in the model was 7 m s^{-1}. Therefore, we tested the uncertainty of the model that results from the variability in *Dv* in the second simulation. The results of these simulations show that the modelled trend would be exaggerated if transport is less (*Dv* = 10^{-5} m^2 s^{-1}). That is, e.g. a larger methane peak is predicted at beginning of fall, which would be smoothed if we were to use a higher *Dv* (10^{-3} m^2 s^{-1}). The best fit to the data is achieved using a *Dv* of 10^{-4} m^2 s^{-1}, which yields a methane concentration of 39 nM in the surface water for the month July, similar to the median of the measurements, 33 nM. A methane concentration of 260 nM is predicted for the bottom water, which is equivalent in magnitude to the median of our measurements, 390 nM.

In order to further evaluate this critical parameter, we estimated *Dv* according to the equation by Osborn (1980):

$$Dv = Kz = \Gamma \frac{\epsilon}{N^2} \quad (8)$$

where Γ is the efficiency of mixing and assumed to be a constant of 0.2. We used published dissipation rates of turbulent kinetic energy (ϵ) in stratified shallow shelf seas (Palmer et al., 2008; Thorpe et al., 2008) and calculated the buoyancy frequency (N) from the available CTD-profiles. The results indicate that *Dv* is in the order of 10^{-4} to 10^{-6} m^2 s^{-1} during stratification. However, this rough approximation neglects hourly changes that can be already of one order of magnitude. For example, Palmer et al. (2008) observed and calculated *Kz* to range between 10^{-4} and 10^{-5} m^2 s^{-1} over a tidal cycle.

After obtaining an appropriate *Dv* (10^{-4} m^2 s^{-1}), which fits best to our methane concentration data, we included methane oxidation in the third model simulation. For this, we subtracted the averaged measured MOx rates from the surface and bottom water reservoirs. MOx was included in the surface water all year round, but in the bottom layer (i.e., in case of stratification) MOx was considered only when sufficient methane has accumulated, that is, for the month May we assume a negligible MOx in the bottom water. The model results do not show any significant difference by comparison to the first simulation (which included only transport) except for the month of June, when the model predicts significant methane consumption by MOx in the bottom water. Due to this decrease of methane concentration in the bottom water, the concentration difference between the surface and bottom water is not as large anymore and less methane is transferred by vertical eddy diffusion into the surface water. The simulation drives the concentration gradient to equilibrium, until the water column becomes fully mixed. We note that the model predicts a similar quantity of methane released to the atmosphere at the beginning of fall whether or not methane oxidation is included in the simulation.

In summary, if *Dv* is below 10^{-4} m^2 s^{-1} over the entire stratification period, then a peak release of methane occurs at the beginning of fall when the water column becomes mixed. Microbial methane oxidation appears insufficient to significantly reduce methane before the gas is transferred into the atmosphere.

The model does not take into account any temporal changes of methane emission. Furthermore, a sensitivity analysis of the model shows that especially wind speed affects model results. 10% higher or lower wind speed over the entire year would in- or decrease the annual flux by 28% or 23%, respectively. Sea surface temperature is less influencing the model result with 1.5% change if the temperature is 10% higher or lower throughout the year.

5 Conclusions

1. Observations at a shallow gas seep site in the central North Sea document methane accumulation below the thermocline during summer stratification, but no methane accumulation in the winter. Similar summer time results are presented by Schneider von Deimling (2011) for the Tommeliten area in the northern North Sea.
2. Our seasonal model bridges our summer and winter field studies and predicts an enhanced sea-air flux at the end of the stratification period. Such an elevated sea-air methane transfer was measured in the Baltic Sea when wind forcing increased after the summer month, breaking down the stratification (Gülzow et al., 2013). The seasonality in fluxes highlights the importance of understanding the effect of seasonal changes on estimates based on short field programs.
3. We show that MOx rates alone cannot be used to characterize the ecosystem microbial activity, as these values are scaled to the methane concentration. We instead propose the use of an average *k'* value of all the data, as an indicator of microbial activity. Such derivation generates a more realistic parameter than values based solely on replicate samples and is similar to values obtained by work-intensive time series incubations.
4. The idea that trapping of methane in the bottom water makes it more available to microbial oxidation could not be verified. Even though the residence time of central North Sea water is about 1.5-2 years (Prandle, 1984; Ursin and Andersen, 1978) and thermal stratification prevails for 4 months and could provide sufficient time to establish a methanotrophic community, we were not able to identify these organisms in the water column. Doubling times of planktonic marine methanotrophs are not known to the authors, as few if any such methanotrophs are currently available in culture. However, if we assume a doubling time of ~10 h as known from cultured methanotrophs (Baani and Liesack, 2008; Khadem et al., 2010) or a doubling time of 3.5 days as was estimated after the Deep Water Horizon incident in the Gulf of Mexico by Kessler et al. (2011), a methanotrophic community could potentially develop in the central North Sea. Even if the doubling time of methanotrophs in the field was even longer as nutrients and substrates can be limiting, still the residence time of the water would permit growth. Possible limitations of essential trace elements or that the methane oxidizing microorganisms are facultative methanotrophs (Tavormina et al., 2013), i.e., not necessarily depending on methane, might explain, why stratification over a summer season of 4 months does not enhance methanotrophy sufficiently to significantly hamper methane release to the atmosphere upon water column mixing.

Author contribution

S. M. designed study, measured methane concentrations and methane oxidation rates, calculated the fluxes, developed the model and carried out model simulations, wrote the manuscript

T.G., R. M., and M.S. deployed the UWMS and post-processed the data

J.-H. K., M. R., H. S., and P. W. collected and post-processed hydroacoustic data

M. T. interpreted methane oxidation rate data, edited manuscript

E. H. implemented and interpreted molecular analyses

Acknowledgement

We are indebted to the captain, crew, and scientific research party of the research vessel *Heincke* (cruise HE406 and HE413), especially to the organizer Sabine Kasten and Gerhard Bohrmann. We like to thank Sven Klüber, Eva Kirschenmann, and Monika Wiebe for their help collecting and analyzing samples on board and in the laboratory. We are grateful to Tessa Clemes from Alfred-Wegener-Institute for Marine and Polar Research (Bremerhaven, Germany), who implemented the microbial analyses. We like to thank Antje Boetius, Gunter Wegener, and Mirja Meiners from the Max Planck Institute for Marine Microbiology (Bremen, Germany) for providing scientific equipment and laboratory support for oxidation rate measurements. This work is part of the DFG project 'Limitations of Marine Methane Oxidation' (MA 3961/2-1).

736 References

737 Baani, M. and Liesack, W.: Two isozymes of particlate methane monooxygenase with different
738 methane oxidation kinetics are found in Methylocystis sp. strain SC2, PNAS, 105, 10203-10208, 2008.
739 Bange, H. W.: Nitrous oxide and methane in European coastal waters, Estuar. Coast. Shelf S., 70, 361-
740 374, 2006.
741 Bange, H. W., Bartell, U. H., Rapsomanikis, S., and Andreae, M. O.: Methane in the Baltic and North
742 Seas and a reassessment of the marine emissions of methane, Global Biogeochem. Cy., 8, 465-480,
743 1994.
744 Bell, R. J., Short, R. T., Van Amerom, F. H. W., and Byrne, R. H.: Calibration of an in situ membrane
745 inlet mass spectrometer for measurements of dissolved gases and volatile organics in seawater,
746 Environ. Sci. Technol., 41, 2007.
747 Bender, M. and Conrad, R.: Kinetics of methane oxidation inoxic soils, Chemosphere, 26, 687-769,
748 1993.
749 Berner, R. A.: Biogeochemical cycles of carbon and sulfur and their effect on atmospheric oxygen
750 over Phanerozoic time, Palaeogeogr. Palaeocl., 73, 97-122, 1989.
751 Boetius, A., Ravenschlag, K., Schubert, C. J., Rickert, D., Widdel, F., Gieskes, A., Amann, R., Jørgensen,
752 B. B., Witte, U., and Pfannkuche, O.: A marine microbial consortium apparently mediating anaerobic
753 oxidation of methane, Nature, 407, 623-626, 2000.
754 Cicerone, R. J. and Oremland, R. S.: Biochemical aspects of atmospheric methane, Global
755 Biogeochem. Cy., 2, 299-327, 1988.
756 Denman, K. L. and Gargett, A. E.: Time and space scales of vertical mixing and advection of
757 phytoplankton in the upper ocean, Limnol. Oceanogr., 28, 801-815, 1983.
758 Eckert, W. and Conrad, R.: Sulfide and methane evolution in the hypolimnion of a subtropical lake: a
759 three-year study, Biogeochemistry, 82, 67-76, 2007.
760 Elsaied, H. E., Hayashi, T., and Naganuma, T.: Molecular analysis of deep-sea hydrothermal vent
761 aerobic methanotrophs by targeting genes of 16S rRNA and particulatemethane monooxygenase,
762 Mar. Biotechnol., 6, 503–509, 2004.
763 Etiope, G., Lassey, K. R., Klusman, R. W., and Boschi, E.: Reappraisal of the fossil methane budget and
764 related emission from geologic sources, Geophys. Res. Lett., 35, L09307, 2008.
765 Ford, P. W., Boon, P. I., and Lee, K.: Methane and oxygen dynamics in a shallow floodplain lake: the
766 significance of period stratification, Hydrobiologia, 485, 97-110, 2002.
767 Gentz, T.: Distribution and fate of methane released from submarine sources – Results of
768 measurements using an improved in situ mass spectrometer, 2013.doctoral thesis, Geosciences,
769 University Bremen, 173 pp., 2013.

Gentz, T., Damm, E., Schneider von Deimling, J., Mau, S., McGinnis, D. F., and Schlüter, M.: A water column study of methane around gas flares located at the West Spitsbergen continental margin, Cont. Shelf Res., doi: 10.1016/j.csr.2013.07.013, 2013. 2013.

Gentz, T. and Schlüter, M.: Underwater cryotrap-membrane inlet system (CT-MIS) for improved in situ analysis of gases, Limnol. Oceanogr.: Methods, 10, 317-328, 2012.

Gerdes, B., Brinkmeyer, R., Dieckmann, G., and Helmke, E.: Influence of crude oil on changes of bacterial communities in Arctic sea-ice, FEMS Microbiol. Ecol., 53, 129-139, 2005.

Grunwald, M., Dellwig, O., Beck, M., Dippner, J. W., Freund, J. A., Kohlmeier, C., Schnetger, B., and Brumsack, H.-J.: Methane in the southern North Sea: Sources, spatial distribution and budgets, Estuar. Coast. Shelf S., 81, 445-456, 2009.

Gülzow, W., Rehder, G., Schneider v. Deimling, J., Seifert, T., and Tóth, Z.: One year of continuous measurements constraining methane emissions from the Baltic Sea to the atmosphere using a ship of opportunity, Biogeosciences, 10, 81-99, 2013.

Holt, J. and Umlauf, L.: Modelling the tidal mixing fronts and seasonal stratification of the Northwest European Continental shelf, Cont. Shelf Res., 28, 887-903, 2008.

Howarth, M. J.: North Sea Circulation. In: Encyclopedia of Ocean Sciences, Steele, J. H. (Ed.), Academic Press, Oxford, 2001.

IPCC: Climate Change 2013 – The Physical Science Basis – Contribution of Working Group I to the Fifth Assessment Report of the Intergovernmental Panel on Climate Change, Cambridge University Press, Cambridge, 2013.

Judd, A. G., Davies, G., Wilson, J., Holmes, R., Baron, G., and Bryden, I.: Contributions to atmospheric methane by natural seepages on the U.K. continental shelf, Mar. Geol., 140, 427-455, 1997.

Kankaala, P., Taipale, S., Nykänen, H., and Jones, R. I.: Oxidation, efflux, and isotopic fractionation of methane during autumnal turnover in a polyhumic, boreal lake, J. Geophys. Res., 112, G02003, 2007.

Kessler, J. D., Valentine, D. L., Redmond, M. C., Du, M., Chan, E. C., Mendes, S. D., Quiroz, E. W., Villanueva, C. J., Shusta, S. S., Werra, L. M., Yvon-Lewis, S. A., and Weber, T. C.: A persistent oxygen anomaly reveals the fate of spilled methane in the deep Gulf of Mexico, Science, 331, 312-315, 2011.

Khadem, A. F., Pol, A., Jetten, M. S. M., and Op den Camp, H. J. M.: Nitrogen fixation by the verrucomicrobial methanotroph '*Methylacidiphilum fumariolicum*' SolV, Microbiology, 156, 1052-1059, 2010.

Killops, S. D. and Killops, V. J.: An Introduction to Organic Geochemistry, Longman, Essex, United Kingdom, 1993.

King, G. M.: Ecological aspects of methane oxidation, a key determinant of global methane dynamics, Adv. Microb. Ecol., 12, 432-468, 1992.

804 Koschel, R.: Untersuchungen zur Phosphataffinitat des Planktons in der euphotischen Zone von Seen,
805 Limnologica, 12, 141-145, 1980.
806 Kröncke, I. and Knust, R.: The Dogger Bank: a special ecological region in the central North Sea,
807 Helgoländer Meeresunters., 49, 335-353, 1995.
808 Largier, J. L.: Considerations in estimating larval dispersal distances from oceanographic data, Ecol.
809 Appl., 13, 71-89, 2003.
810 Mau, S., Blees, J., Helmke, E., Niemann, H., and Damm, E.: Vertical distribution of methane oxidation
811 and methanotrophic response to elevated methane concentrations in stratified waters of the Arctic
812 fjord Storfjorden (Svalbard, Norway), Biogeosciences, 10, 6267–6278, 2013.
813 Mau, S., Heintz, M. B., and Valentine, D. L.: Quantification of CH_4 loss and transport in dissolved
814 plumes of the Santa Barbara Channel, California, Cont. Shelf Res., 32, 110-120, 2012.
815 McDonald, I. R., Bodrossy, L., Chen, Y., and Murrell, J. C.: Molecular ecology techniques for the study
816 of aerobic methanotrophs, Appl. Environ. Microb., 74, 1305-1315, 2008.
817 McDonald, I. R. and Murrell, J. C.: The particulate methane monooxygenase gene pmoA and its use as
818 a functional gene probe for methanotrophs, FEMS Microbiol. Lett., 156, 205-210, 1997.
819 McGillis, W., R., Edson, J., B., Ware, J., D., Dacey, J., W. H., Hare, J., E., Fairall, C., W., and Wanninkhof,
820 R.: Carbon dioxide flux techniques performed during GasEx-98, Mar. Chem., 75, 267-280, 2001.
821 McGinnis, D. F., Greinert, J., Artemov, Y., Beaubien, S. E., and Wuest, A.: Fate of rising methane
822 bubbles in stratified waters: How much methane reaches the atmosphere?, J. Geophys. Res., 111, 15,
823 2006.
824 Muyzer, G., de Waal, E., and Uitterlinden, A.: Profiling of complex microbial populations by
825 denaturing gradient gel electrophoresis analysis of polymerase chain reaction-amplified genes coding
826 for 16S rRNA, Appl. Environ. Microbiol., 59, 695-700, 1993.
827 Narvenkar, G., Naqvi, S. W. A., Kurian, S., Shenoy, D. M., Pratihary, A. K., Naik, H., Patil, S., Sarkar, A.,
828 and Gauns, M.: Dissolved methane in Indian freshwater reservoirs, Environ. Monit. Assess., 185,
829 6989–6999, 2013.
830 Niemann, H., Elvert, M., Hovland, M., Orcutt, B., Judd, A. G., Suck, I., Gutt, J., Joye, S., Damm, E.,
831 Finster, K., and Boetius, A.: Methane emission and consumption at a North Sea gas seep (Tommeliten
832 area), Biogeosciences 2, 335-351, 2005.
833 Osborn, T. R.: Estimates of the local rate of diffusion from dissipation measurements, J. Phys.
834 Oceanogr., 10, 83-89, 1980.
835 Otto, L., Zimmermann, J. T. F., Furnes, G. K., Mork, M., Saetre, R., and Becker, G.: Review of the
836 physical oceanography of the North Sea, Neth. J. Sea Res., 26, 161-238, 1990.

Pack, M. A., Heintz, M. B., Reeburgh, W. S., Trumbore, S. E., Valentine, D. L., Xu, X., and Druffel, E. R. M.: A method for measuring methane oxidation rates using low-levels of ^{14}C-labeled methane and accelerator mass spectrometry, Limnol. Oceanogr.: Methods, 9, 245-260, 2011.

Palmer, M. R., Rippeth, T. P., and Simpson, J. H.: An investigation of internal mixing in a seasonally stratified shelf sea, J. Geophys. Res., 113, 2008.

Pingree, R. D. and Griffiths, D. K.: Tidal Fronts on the Shelf Seas Around the British Isles, J. Geophys. Res., 83, 4615-4622, 1978.

Prandle, D.: A modelling study of the mixing of ^{137}Cs in the seas of the European continental shelf, Philos. T. Roy. Soc. A 310, 407-436, 1984.

Pruesse, E., Peplies, J., and Glöckner, F. O.: SINA: accurate high-throughput multiple sequence alignment of ribosomal RNA genes, Bioinformatics, 28, 1823-1829, 2012.

Reeburgh, W. S., Ward, B. B., Whalen, S. C., Sandbeck, K. A., Kilpatrick, K. A., and Kerkhof, L. J.: Black Sea methane geochemistry, Deep-Sea Res., 38, S1189-S1210, 1991.

Rehder, G., Keir, R. S., Suess, E., and Pohlmann, T.: The multiple sources and patterns of methane in North Sea waters, Aquat. Geochem., 4, 403-427, 1998.

Schlüter, M. and Gentz, T.: Application of membrane inlet mas spectrometry for online and in situ analysis of methane in aquatic environments, J. Am. Soc. Mass Spectrom., 19, 1395-1402, 2008.

Schneider von Deimling, J., Rehder, G., Greinert, J., McGinnis, D. F., Boetius, A., and Linke, P.: Quantification of seep-related methane gas emissions at Tommeliten, North Sea, Cont. Shelf Res., 31, 876-878, 2011.

Schroot, B. M., Klaver, G. T., and Schuettenhelm, T. E.: Surface and subsurface expressions of gas seepage to the seabed - examples from the southern North Sea, Mar. Petrol. Geol., 22, 499-515, 2005.

Scranton, M. I. and McShane, K.: Methane fluxes in the southern North Sea: The role of European rivers, Cont. Shelf Res., 11, 37-52, 1991.

Short, R. T., Fries, D. P., Kerr , M. L., Lembke, C. E., Toler, S. K., Wenner, P. G., and Byrne, R. H.: Underwater mass spectrometers for in situ chemical analysis of the hydrosphere, J. Am. Soc. Mass Spectrom., 12, 676-682, 2001.

Sundermeyer, M. A. and Price, J. F.: Lateral mixing and the North Atlantic tracer release experiment: observations and numerical simulations of Lagrangian particles and a passive tracer, J. Geophys. Res., 103, 21481-21497, 1998.

Sündermann, J. and Pohlmann, T.: A brief analysis of North Sea physics, Oceanologia, 53, 663-689, 2011.

Tavormina, P. L., Ussler III, W., and Orphan, V. J.: Planktonic and sediment-associated aerobic methanotrophs in two seep systems along the North American Margin, Appl. Environ. Microbiol., 74, 3985-3995, 2008.

Tavormina, P. L., Ussler, W., Steele, J. A., Connon, S. A., Klotz, M. G., and Orphan, V. J.: Abundance and distribution of diverse membrane-bound monooxygenase (Cu-MMO) genes within the Costa Rica oxygen minimum zone, Environmental microbiology reports, 5, 414-423, 2013.

Thorpe, S. A., Green, J. A. M., Simpson, J. H., Osborn, T. R., and Nimmo Smith, W. A. M.: Boils and turbulences in a weakly stratified shallow tidal sea, J. Phys. Oceanogr., 38, 1711-1730, 2008.

Ursin, E. and Andersen, K. P.: A model of the biological effects of eutrophication in the North Sea, Rapp. P.-v. Reun. Cons. Int. Explor. Mer, 172, 366-377, 1978.

Valentine, D. L.: Emerging topics in marine methane biogeochemistry, Annu. Rev. Mar. Sci., 3, 147-171, 2011.

Valentine, D. L., Blanton, D. C., Reeburgh, W. S., and Kastner, M.: Water column methane oxidation adjacent to an area of active hydrate dissociation, Eel River Basin, Geochim. Cosmochim. Ac., 65, 2633-2640, 2001.

Valentine, D. L., Kessler, J. D., Redmond, M. C., Mendes, S. D., Heintz, M. B., Farwell, C., Hu, L., Kinnaman, F. S., Yvon-Lewis, S., Du, M., Chan, E. W., Tigreros, F. G., and Villanueva, C. J.: Propane respiration jump-starts microbial response to a deep oil spill, Science, 330, 208-211, 2010.

Wasmund, K., Kurtboke, D. I., Burns, K. A., and Bourne, D. G.: Microbial diversity in sediments associated with a shallow methane seep in the tropical Timor Sea of Australia reveals a novel aerobic methanotroph diversity, FEMS Microbiol. Ecol., 68, 142–151, 2009.

Wenner, P. G., Bell, P. G., van Amerom, F. H. W., Toler, S. K., Edkins, J. E., Hall, M. L., Koehn, K., Short, R. T., and Byrne, R. H.: Environmental chemical mapping using an underwater mass spectrometer, Trac-Trend Anal. Chem., 23, 288-295, 2004.

Wiesenburg, D. A. and Guinasso, J. N. L.: Equilibrium solubilities of methane, carbon monoxide, and hydrogen in water and sea water, J. Chem. Eng. Data, 24, 356-360, 1979.

Wunsch, C. and Ferrari, R.: Vertical mixing, energy, and the general circulation of the oceans, Annu. Rev. Fluid Mech., 36, 281-314, 2004.

Tables

Tab. 1 Classification of partial 16S rRNA gene sequences (Fig. 7) to bacterial taxa performed with the Silva classifier (Pruesse et al., 2012). The confidence value (0–1) for assignment at the level of class and genus is given in parentheses.

No.	Class	Family
1	Alphaproteobacteria (0.4)	*SAR11 clade* (0.2)
2	Cyanobacteria (1)	*Chloroplast* (1)
3	Alphaproteobacteria (1)	*Rhodobacteraceae* (1)
4	Bacteroidetes incertae sedis (0.43)	*Marinifilum* (0.4)
5	Alphaproteobacteria (1)	*Rhodobacteraceae* (1)
6	Alphaproteobacteria (1)	*Rhodobacteraceae* (1)
7	Alphaproteobacteria (1)	*Rhodobacteraceae* (1)
8	Cyanobacteria (1)	*Synechococcus* (1)
9	Cyanobacteria (1)	*Synechococcus* (1)
10	Gammaproteobacteria (1)	*Pseudoalteromonadaceae* (1)
11	Proteobacteria (0.36)	
12	Alphaproteobacteria (1)	*Rhodospirillaceae* (0.8)
13	Alphaproteobacteria (0.91)	*Rhodospirillaceae* (0.7)

925 Tab. 2 Comparison of highest methane concentrations, methane oxidation rates, and sea-air fluxes from different locations

Location	**Methane concentration**	**MOx-rate**	**SAF**	**Reference**
	up to nM	*nM day^{-1}*	*nmol m^{-2} s^{-1}*	
Seep sites				
central North Sea	1628	0.04-840	0.02-8.3	this study
Coal Oil Point, Santa Barbara Basin	1900	0.02-30	1.8	Mau et al., 2012; Pack et al., 2011
Tommeliten, North Sea	268		10.8*	Schneider von Deimling et al., 2011
west of Prins Karls Forland, Svalbard	524	up to 0.8		Gentz et al., 2013
Eel River Basin	300	0.002-0.8		Valentine et al., 2001
Deepwater Horizon event				
Gulf of Mexico	180000	up to 820		Valentine et al., 2010
Gulf of Mexico	1000000	up to 5900		Crespo-Medina et al., 2014
Overall areas				
Baltic Sea	38		0.008-0.2	Gülzow et al., 2013
Southern Bight of the North Sea	372	0.0002-0.3	0.07-7	Scranton and McShane (1991)
general European shelf estimate	21		0.11-0.24	Bange, 2006
Lakes				
floodplain lake in south-eastern Australia	50000		8.3-2700	Ford et al., 2002
polyhumic lake in southern Finland	150000	30-14400	0.5-695	Kankaala et al., 2007
the subtropical Lake Kinneret in Israel	450000			Eckert and Conrad, 2007
freshwater reservoirs in India	156000			Narvenkar et al., 2013

*direct transport via bubbles

926

927

928 Figures

929 Fig. 1: Location of the study area in the central North Sea. The main currents are shown following
930 Howarth (2001). The map was drawn using GeoMapApp with 40 m contours.

931

932 Fig. 2: Overview of gas flares mapped in January 2014 and CTD stations sampled in July 2013 (S12-
933 S21) and January 2014 (W2-W12). Flares cluster in 5 distinct areas (cluster 1-5) and reach to 6 m
934 from the sea surface (e.g. cluster 2 in upper right insert), which corresponds to the echosounder's
935 transducer depth. Hence, most likely the gas transport extends to the sea surface. Cluster 1
936 corresponds to the gas seep area investigated by Gentz (2013) (lower right insert).

937

938 Fig. 3: Depth profiles of potential temperature, salinity, density (sigma theta), and oxygen for all
939 stations in both summer and winter field programs.

940

941 Fig. 4: A-B Contour plots of the dissolved methane concentrations measured in the water column in
942 July 2013 and January 2014. The 6 km transect was divided into an eastern (positive numbers) and
943 western part (negative numbers) starting from the center station at 0 km. Note the different
944 methane concentration scales, which are necessary to properly display the different concentration
945 ranges. The black dots indicate the sampled water depths.

946

947 Fig. 5: Box plot of methane concentrations recorded by UWMS on 21.07.2013. The times on the right
948 side refer to the start and end times of the rectangular transects the UWMS was towed along in the
949 vicinity of flare cluster 1 (Fig. 2) at each water depth. Profiles obtained with UWMS are consistent
950 with discrete water sampling data.

951

952 Fig. 6: A-C Methane oxidation rates versus water depth measured with ^{3}H-methane in July 2013 (A),
953 with ^{3}H-methane in January 2014 (B), and using ^{14}C-methane as tracer in July 2013 (C). D Time series
954 of water samples collected during both field programs and incubated with ^{3}H-methane.

955

956 Fig. 7: DGGE profile of 16S rRNA gene fragments of samples from different depth and stations in the
957 central North Sea. Numbers on the lines indicate excised and successfully sequenced DGGE bands,
958 whose phylogenetic assignment is listed in Tab. 1.

959

960 Fig. 8: Methane oxidation rate versus methane concentration. A Michaelis Menten kinetics of Eq. 7
961 (MM-kinetics) using the parameters v_{max}=1000 nM day^{-1} and K_m=800 nM for curve MM-kinetics 1 and
962 v_{max}=100 nM day^{-1} and K_m=12000 nM for curve MM-kinetics 2. Together, both curves encompass the

963 range of the enzyme kinetics available. B Close up of the data for MOx-rates < 20 nM day^{-1} and MM-
964 kinetics 2 in that range and the linear regression of all data (R^2=0.82).
965
966 Fig. 9: Sketch of transport and loss terms estimated for the study area in nmol m^{-2} s^{-1}.
967
968 Fig. 10: Model results over the course of a year. The mixed layer depth (D) shows the time period of
969 water column stratification from May until August. The mixed layer deepens during this time until
970 the entire water column is mixed again. During stratification, the water column is separated in
971 surface (B) and bottom water (C) whereas during the rest of the year the entire water column is well
972 mixed with methane concentrations shown in B. A displays the sea-air flux based on monthly mean
973 wind speed derived from the stations shown in Fig. 1. Model simulations including solely vertical
974 transport processes are shown as gray to black lines, which illustrate the range due to different D_v
975 values (see text). The model simulation based on methane oxidation in addition to vertical transport
976 is shown as a red line.

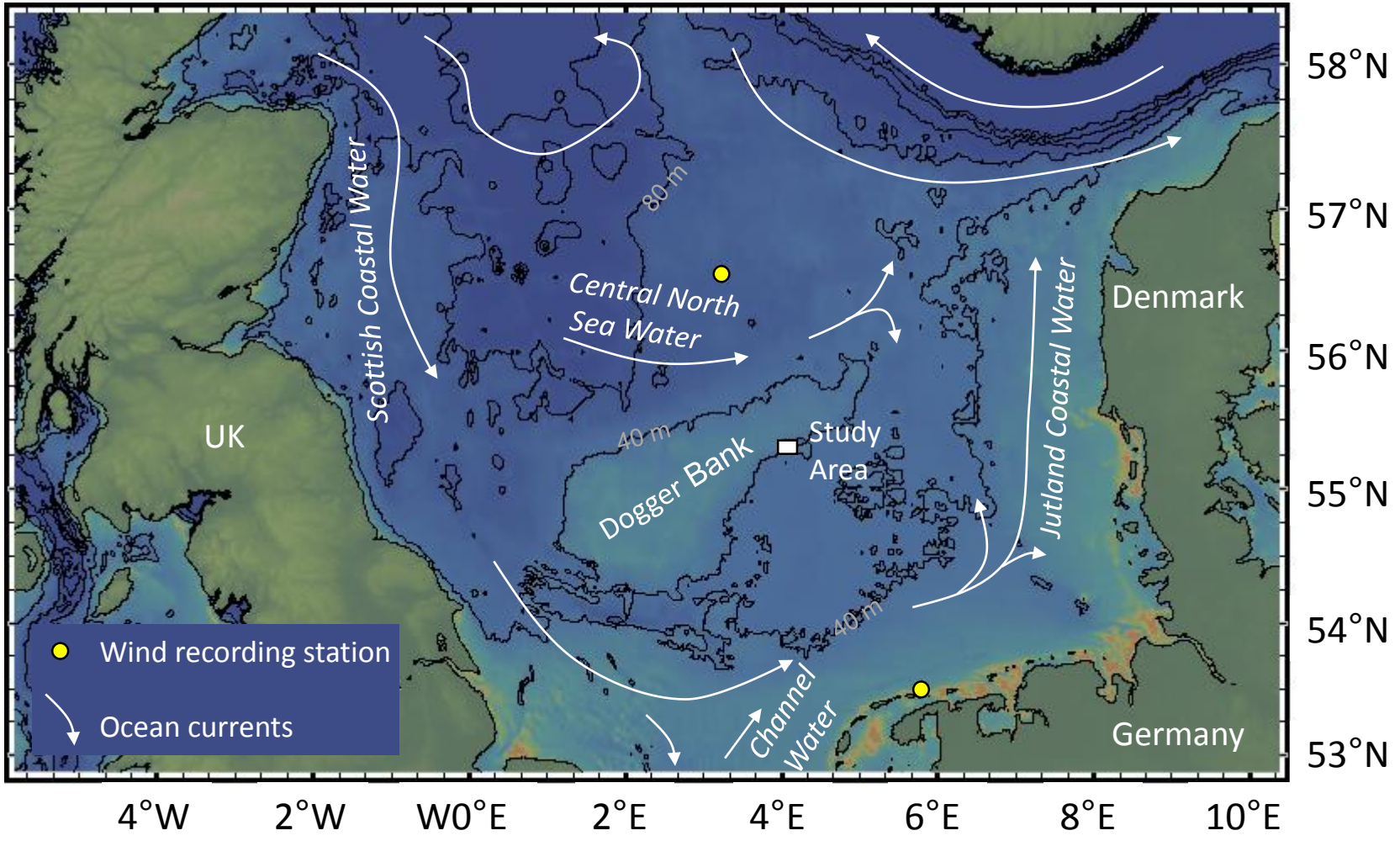

Fig. 1: Location of the study area in the central North Sea. The main currents are shown following Howarth (2001). The map was drawn using GeoMapApp with 40 m contours.

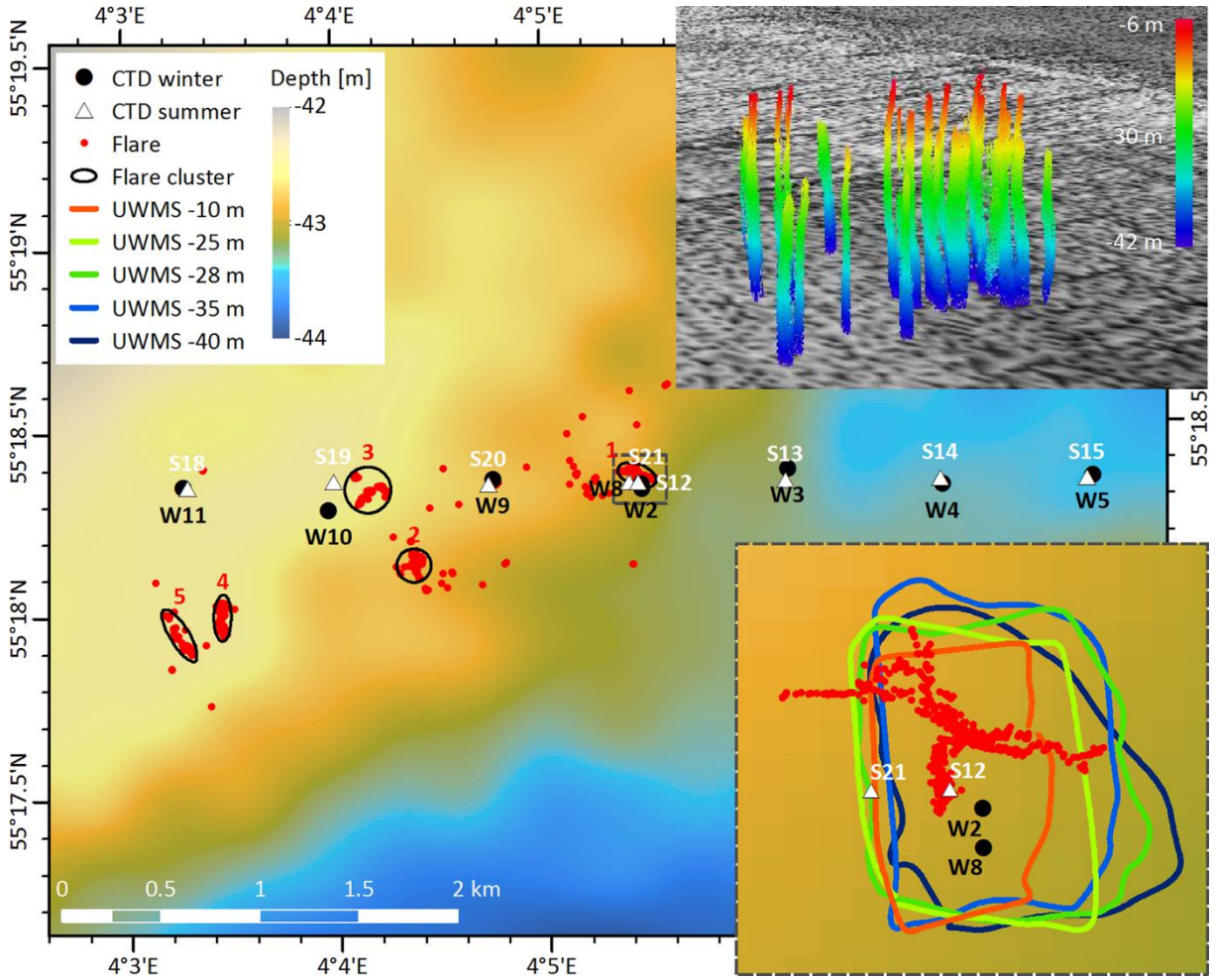

Fig. 2: Overview of gas flares mapped in January 2014 and CTD stations sampled in July 2013 (S12-S21) and January 2014 (W2-W12). Flares cluster in 5 distinct areas (cluster 1-5) and reach to 6 m from the sea surface (e.g. cluster 2 in upper right insert), which corresponds to the echosounder's transducer depth. Hence, most likely the gas transport extends to the sea surface. Cluster 1 corresponds to the gas seep area investigated by Gentz (2013) (lower right insert).

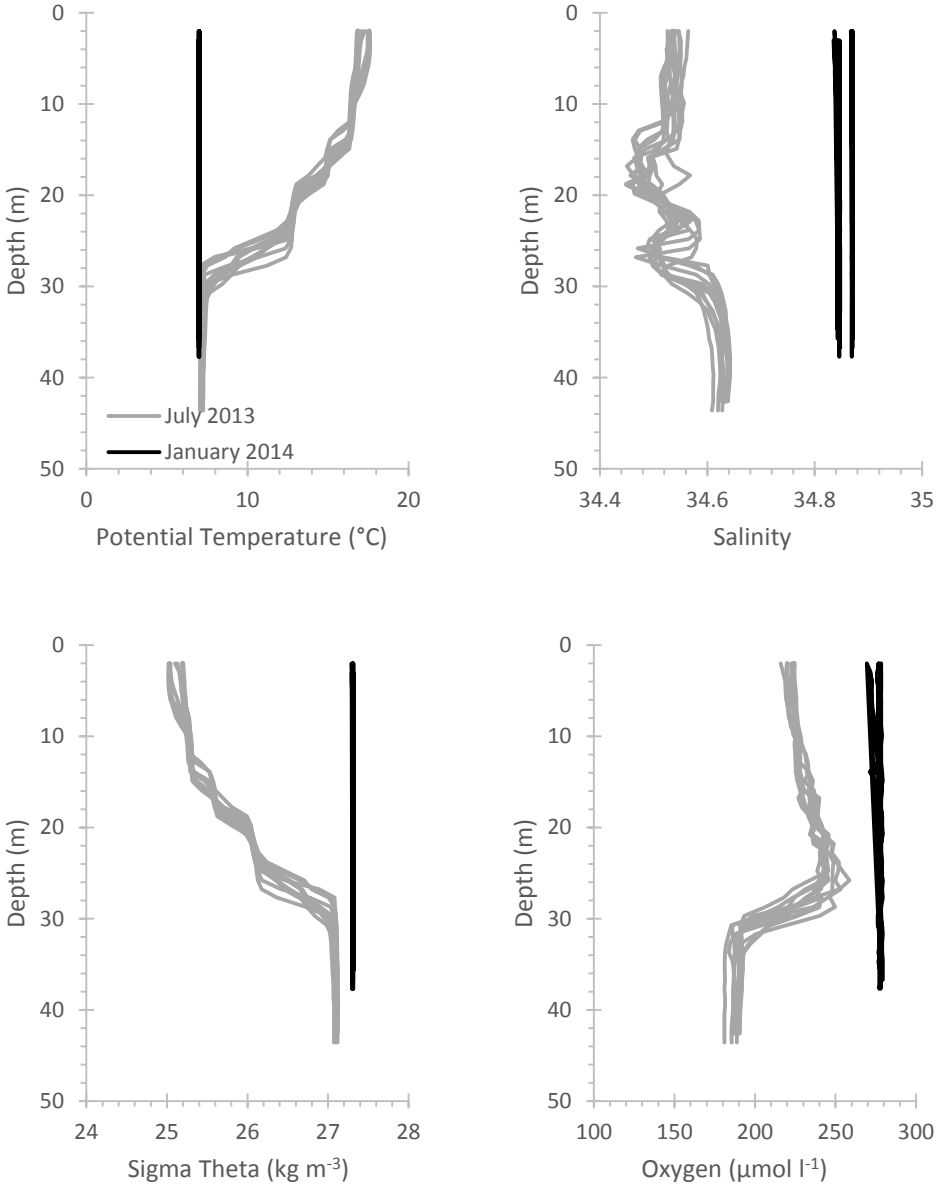

Fig. 3: Depth profiles of potential temperature, salinity, density (sigma theta), and oxygen for all stations in both summer and winter field programs.

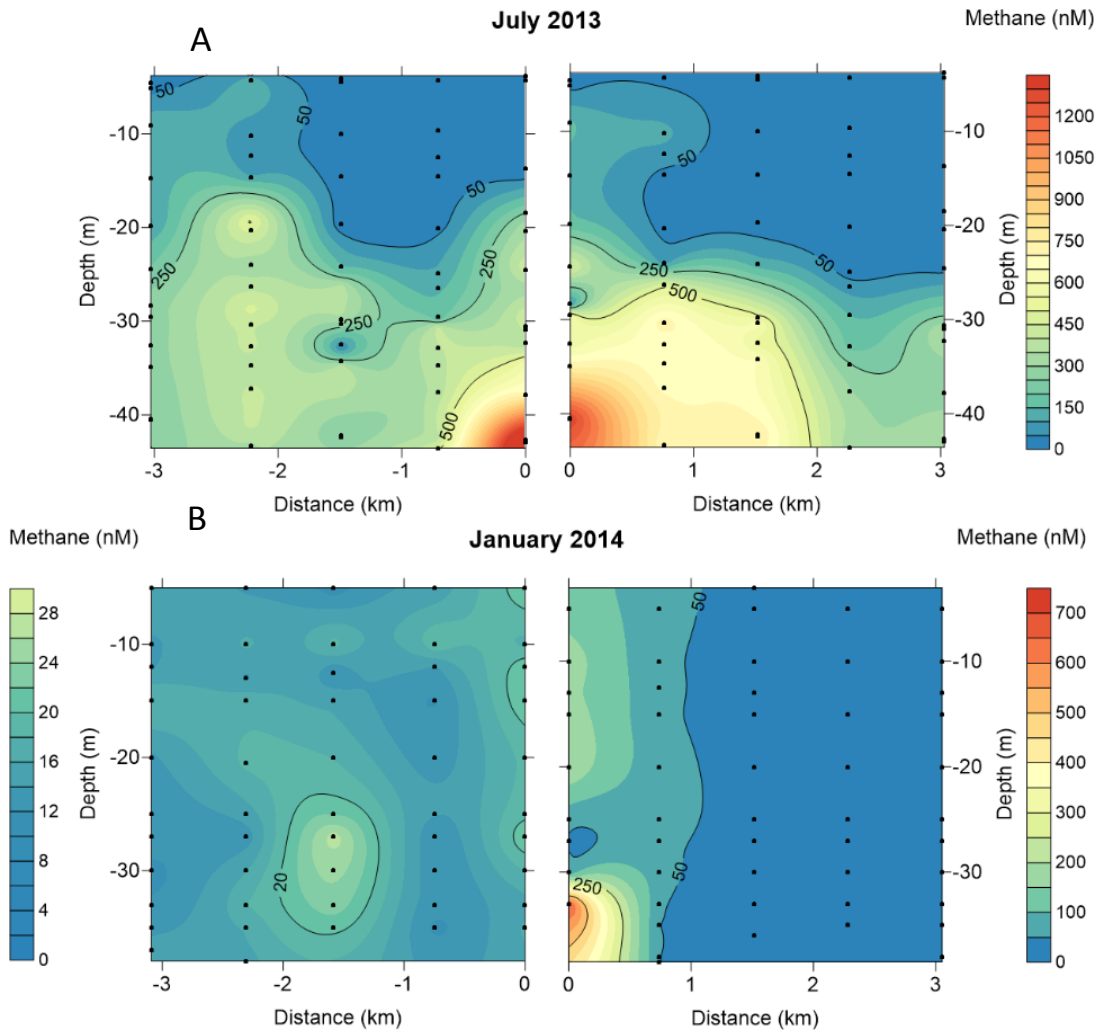

Fig. 4: A-B Contour plots of the dissolved methane concentrations measured in the water column in July 2013 and January 2014. The 6 km transect was divided into an eastern (positive numbers) and western part (negative numbers) starting from the center station at 0 km. Note the different methane concentration scales, which are necessary to properly display the different concentration ranges. The black dots indicate the sampled water depths.

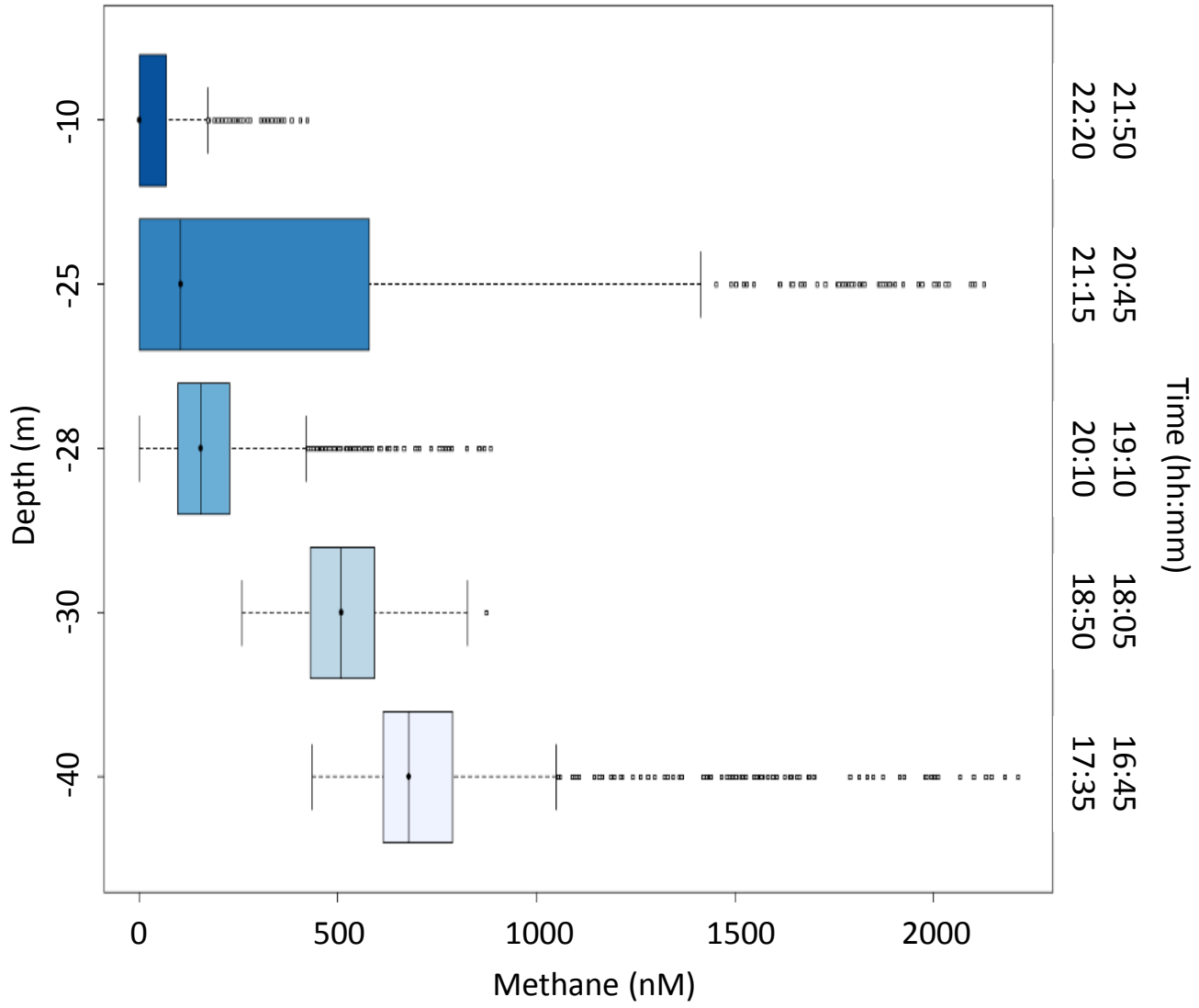

Fig. 5: Box plot of methane concentrations recorded by UWMS on 21.07.2013. The times on the right side refer to the start and end times of the rectangular transects the UWMS was towed along in the vicinity of flare cluster 1 (Fig. 2) at each water depth. Profiles obtained with UWMS are consistent with discrete water sampling data.

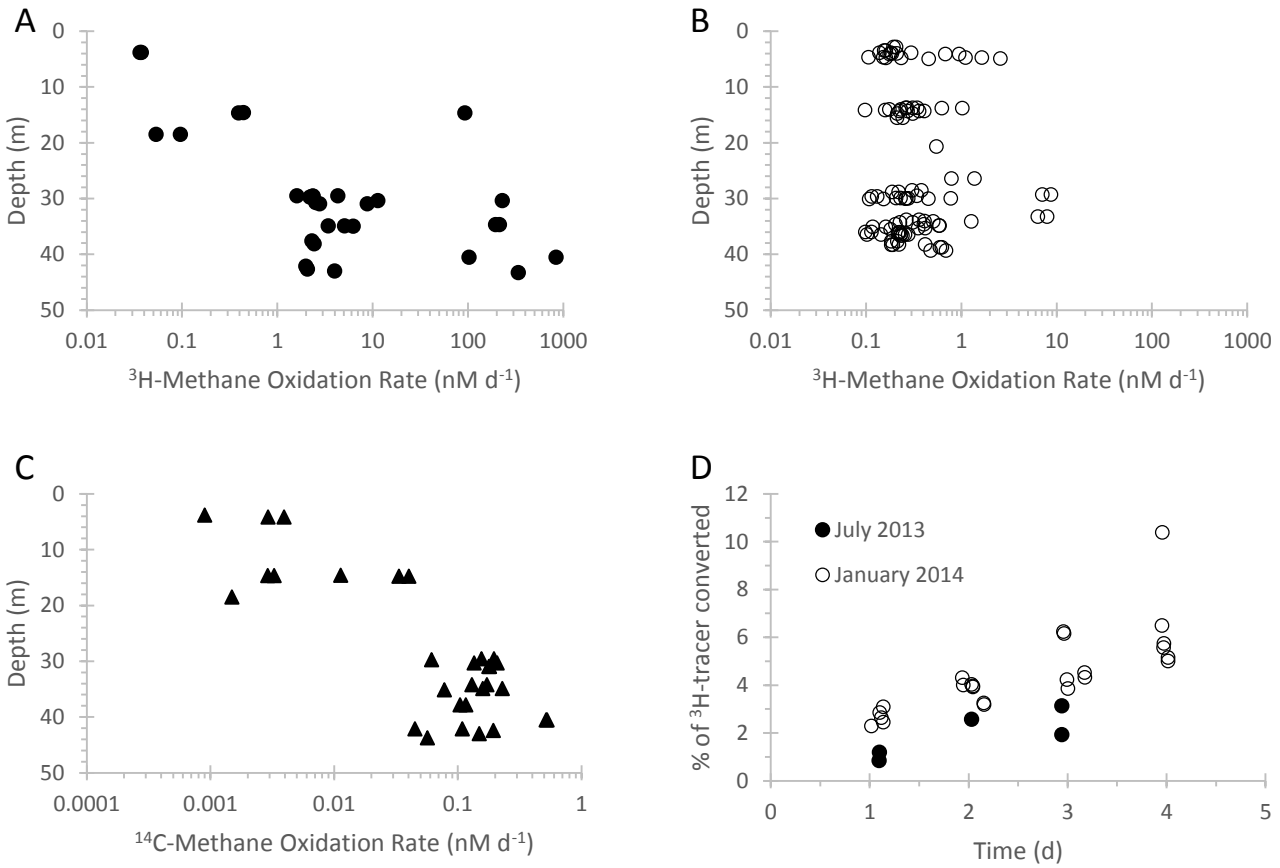

Fig. 6: A-C Methane oxidation rates versus water depth measured with ^{3}H-methane in July 2013 (A), with ^{3}H-methane in January 2014 (B), and using ^{14}C-methane as tracer in July 2013 (C). D Time series of water samples collected during both field programs and incubated with ^{3}H-methane.

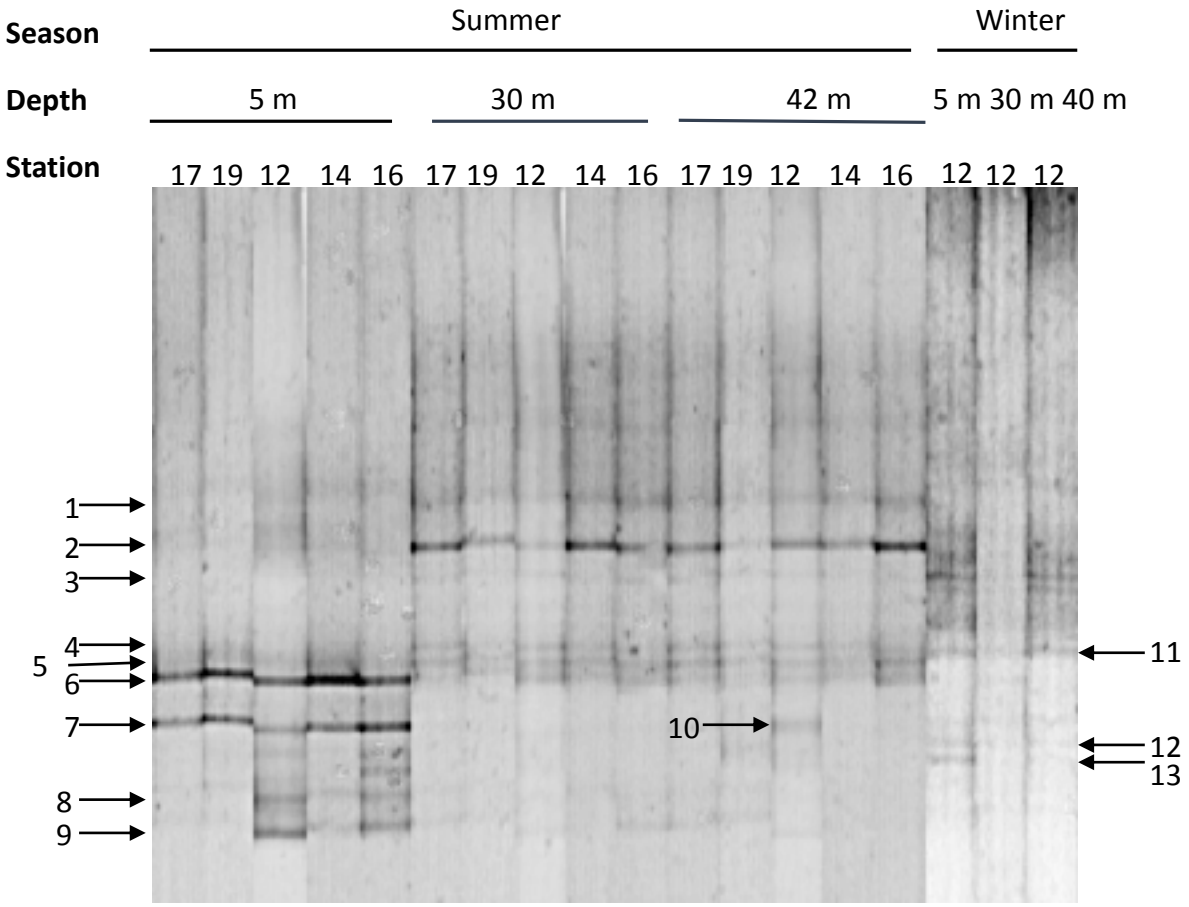

Fig. 7: DGGE profile of 16S rRNA gene fragments of samples from different depth and stations in the central North Sea. Numbers on the lines indicate excised and successfully sequenced DGGE bands, whose phylogenetic assignment is listed in Tab. 1.

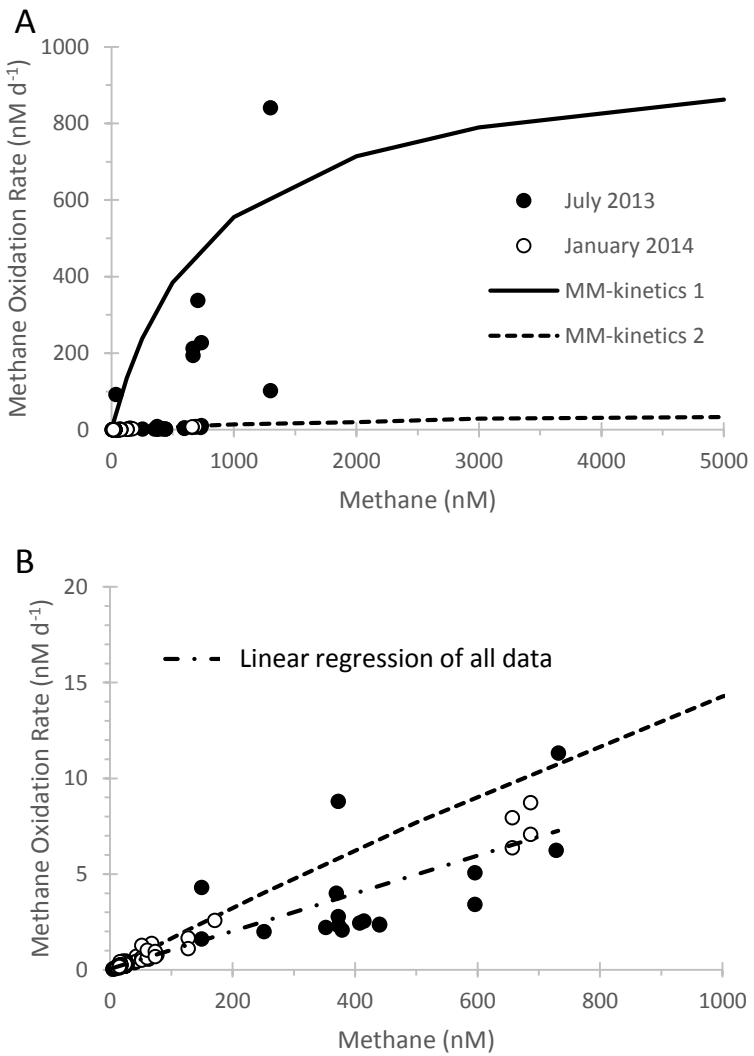

Fig. 8: Methane oxidation rate versus methane concentration. A Michaelis Menten kinetics of Eq. 7 (MM-kinetics) using the parameters v_{max}=1000 nM day^{-1} and K_m=800 nM for curve MM-kinetics 1 and v_{max}=100 nM day^{-1} and K_m=12000 nM for curve MM-kinetics 2. Together, both curves encompass the range of the enzyme kinetics available. B Close up of the data for MOx-rates < 20 nM day^{-1} and MM-kinetics 2 in that range and the linear regression of all data (R^2=0.82).

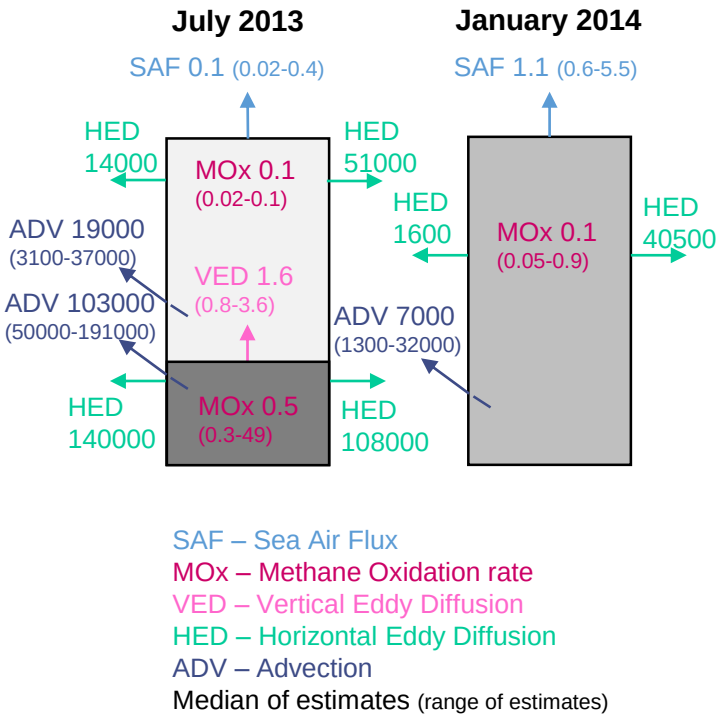

Fig. 9: Sketch of transport and loss terms estimated for the study area in nmol m^{-2} s^{-1}.

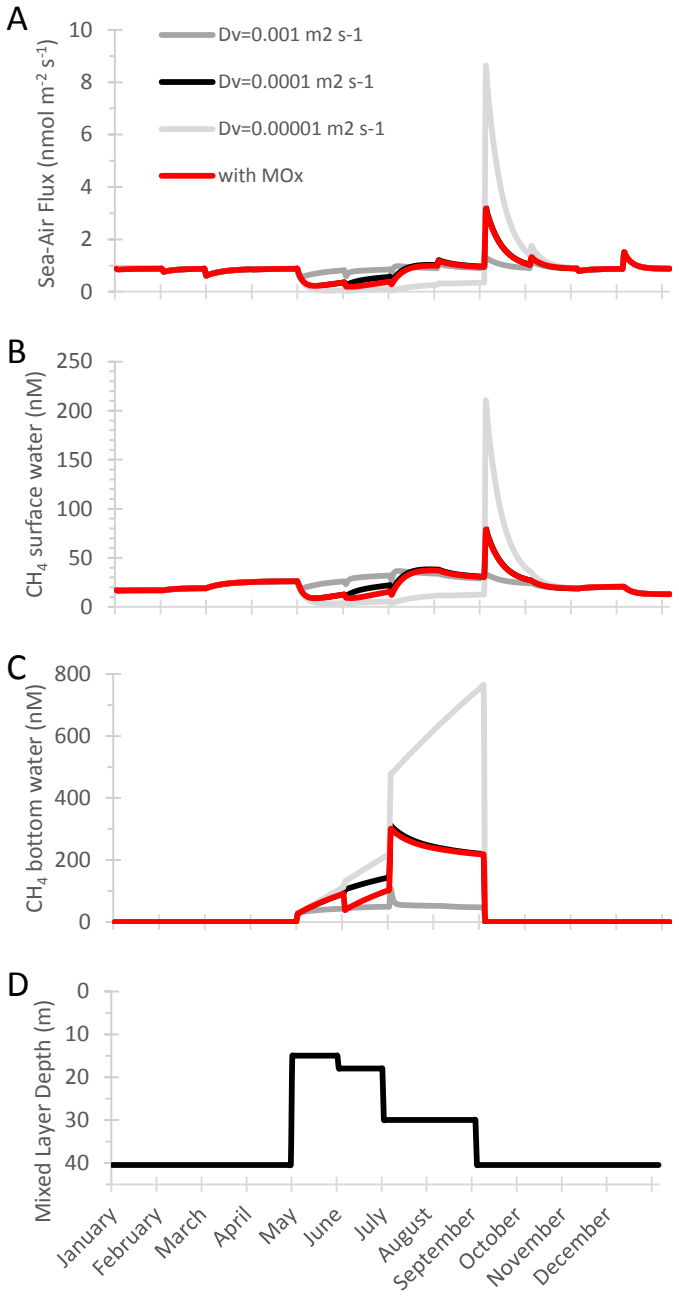

Fig. 10: Model results over the course of a year. The mixed layer depth (D) shows the time period of water column stratification from May until August. The mixed layer deepens during this time until the entire water column is mixed again. During stratification, the water column is separated in surface (B) and bottom water (C) whereas during the rest of the year the entire water column is well mixed with methane concentrations shown in B. A displays the sea-air flux based on monthly mean wind speed derived from the stations shown in Fig. 1. Model simulations including solely vertical transport processes are shown as gray to black lines, which illustrate the range due to different D_v values (see text). The model simulation based on methane oxidation in addition to vertical transport is shown as a red line.